HHS Public Access

Author manuscript

Cell Rep. Author manuscript; available in PMC 2020 September 01.

Published in final edited form as:

Cell Rep. 2020 August 11; 32(6): 108007. doi:10.1016/j.celrep.2020.108007.

Runx2+ Niche Cells Maintain Incisor Mesenchymal Tissue Homeostasis through IGF Signaling

Shuo Chen[1,2], **Junjun Jing**[1], **Yuan Yuan**[1], **Jifan Feng**[1], **Xia Han**[1], **Quan Wen**[1], **Thach-Vu Ho**[1], **Chelsea Lee**[3], **Yang Chai**[1,4,*]

[1]Center for Craniofacial Molecular Biology, University of Southern California, Los Angeles, CA 90033, USA

[2]Department of Oral and Maxillofacial Surgery, Peking University School and Hospital of Stomatology, Beijing 100081, China

[3]Eli and Edythe Broad CIRM Center for Regenerative Medicine and Stem Cell Research, University of Southern California, Los Angeles, CA 90033, USA

[4]Lead Contact

SUMMARY

Stem cell niches provide a microenvironment to support the self-renewal and multi-lineage differentiation of stem cells. Cell-cell interactions within the niche are essential for maintaining tissue homeostasis. However, the niche cells supporting mesenchymal stem cells (MSCs) are largely unknown. Using single-cell RNA sequencing, we show heterogeneity among Gli1+ MSCs and identify a subpopulation of Runx2+/Gli1+ cells in the adult mouse incisor. These Runx2+/Gli1+ cells are strategically located between MSCs and transit-amplifying cells (TACs). They are not stem cells but help to maintain the MSC niche via IGF signaling to regulate TAC proliferation, differentiation, and incisor growth rate. ATAC-seq and chromatin immunoprecipitation reveal that Runx2 directly binds to Igfbp3 in niche cells. This Runx2-mediated IGF signaling is crucial for regulating the MSC niche and maintaining tissue homeostasis to support continuous growth of the adult mouse incisor, providing a model for analysis of the molecular regulation of the MSC niche.

In Brief

Chen et al. show that Runx2+/Gli1+ niche cells in the adult mouse incisor coordinate the transition from mesenchymal stem cell to transit-amplifying cell (TAC) and control the growth rate of incisors. Runx2 regulates Igfbp3 to control IGF signaling, determine the fate of TACs, and maintain incisor mesenchymal tissue homeostasis.

*Correspondence: ychai@usc.edu.

AUTHOR CONTRIBUTIONS

Conceptualization, S.C. and Y.C.; Methodology, S.C., J.J., Y.Y., and X.H.; Investigation, S.C., X.H., J.F., and Q.W.; Data Collection & Analysis, S.C., T.-V.H., C.L., and Y.C.; Writing – Review & Editing, S.C., J.J., Y.Y., J.F., and Y.C.; Funding Acquisition, Y.C.

DECLARATION OF INTERESTS

The authors declare no competing interests.

SUPPLEMENTAL INFORMATION

Supplemental Information can be found online at https://doi.org/10.1016/j.celrep.2020.108007.

Graphical Abstract

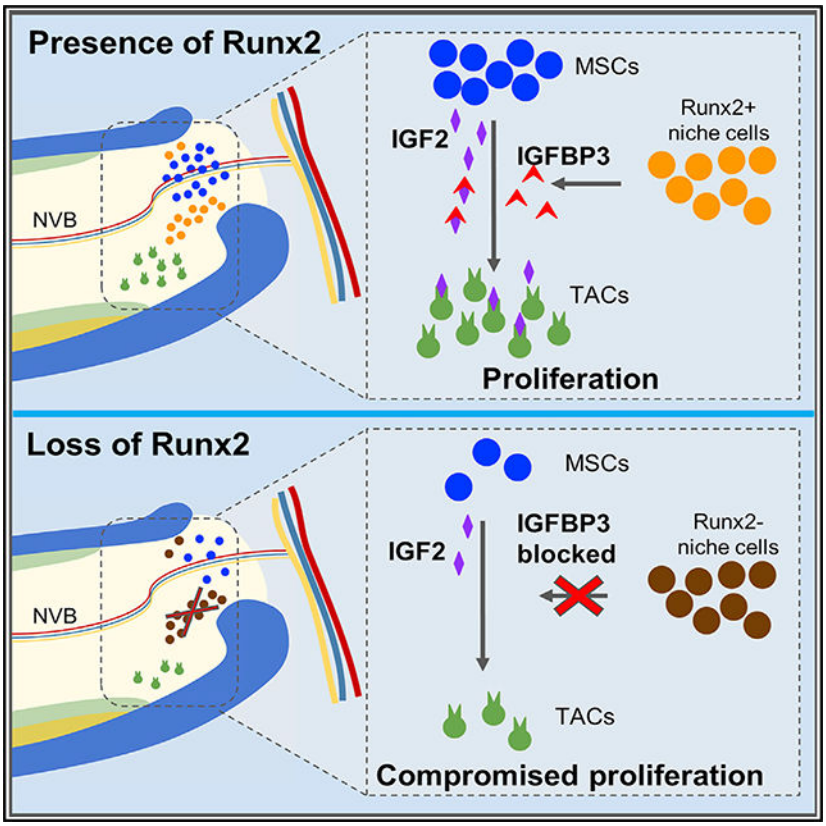

INTRODUCTION

Continuous cell replacement helps to maintain homeostasis in tissues such as the skin and gastrointestinal tract (Blanpain and Fuchs, 2014; Kaukua et al., 2014). Tissue homeostasis is supported by stem cells, which reside within specialized microenvironments, called niches, that in turn provide support and signals to regulate stem cell self-renewal and differentiation (Chacón-Martínez et al., 2018; Rezza et al., 2016; Simons and Clevers, 2011). The complex dynamics of the stem cell niche are orchestrated by the supporting extracellular matrix (ECM), niche cells, and soluble signaling factors that act via autocrine or paracrine mechanisms (Morrison and Spradling, 2008; Scadden, 2014). Several well-defined niches harbor stem cells necessary to maintain homeostasis and regenerate tissues after damage. The intestinal epithelium, for example, contains Paneth cells that secrete niche signals such as Wnt3, Egf, and Notch ligand Dll4 to intestinal stem cells (Ganz, 2000; Sato et al., 2011). In the hair follicle epidermis, transit-amplifying cells (TACs) crucially help regulate the stem cell niche by producing Sonic hedgehog (Shh) (Hsu et al., 2014). In the mesenchyme, however, niche cells for mesenchymal stem cells (MSCs) have yet to be well defined.

Mammalian teeth harbor MSCs in dental pulp that contribute to tooth homeostasis and repair. In particular, rodent incisors provide an excellent window into the activities of MSCs and their niches, because these teeth continue to grow throughout the animal’s life

(Lapthanasupkul et al., 2012; Wang et al., 2007). MSC and TAC populations can be clearly identified in the proximal region of the rodent incisor, residing between the labial and the lingual sides of the epithelial cervical loop (Sharpe, 2016; Shi et al., 2019; Zhao et al., 2014). Recently, using genetic lineage tracing, several markers have been identified as labeling different MSC populations *in vivo* (An et al., 2018b; Feng et al., 2011; Kaukua et al., 2014; Zhao et al., 2014), improving our understanding of the heterogeneity of stem cell populations. Specifically, our previous study has shown that quiescent Gli1+ cells are typical MSCs in the mouse incisor. These stem cells surround the neurovascular bundle in the proximal region of the incisor. This population of MSCs continuously gives rise to TACs, which actively divide and then differentiate into odontoblasts and dental pulp cells to support both homeostasis and injury repair (Zhao et al., 2014). Kaukua and colleagues showed that Plp1/Sox10+ glia-derived MSCs dwell in a niche in the proximal region of the mouse incisor (Kaukua et al., 2014). Although Gli1+ MSCs contribute to the entire dental pulp, these multipotent Plp1/Sox10+ Schwann cell precursors (SCPs) and Schwann cells contribute to approximately half of the pulp cells and odontoblasts during development, growth, and regeneration of the incisor (Kaukua et al., 2014). Another study identified an MSC population derived from neuronal glia; it reported a subpopulation of MSCs that express CD90/Thy1 and contribute to 30% of differentiated cell progeny during incisor eruption and injury repair (An et al., 2018b). Collectively, these studies suggest there may be considerable heterogeneity among MSCs in the adult mouse incisor.

Runx2 encodes a transcription factor that is known for its important role during bone and tooth development. In humans, *RUNX2* mutations are responsible for an autosomal dominant disorder, cleidocranial dysplasia (CCD), which is associated with bone formation defects (Jaruga et al., 2016; Wang et al., 2013). Disruption of *Runx2* in mice leads to maturational arrest of osteoblasts and therefore a complete lack of ossification during both endochondral and intramembranous bone formation, whereas tooth morphogenesis is arrested at the cap stage (D'Souza et al., 1999; Komori et al., 1997; Otto et al., 1997). In the dental mesenchyme, *Runx2* regulates mesenchymal odontogenic activity by modulating antagonistic interaction between transcription factors Msx1 and Osr2, and plays an essential role in upregulating mesenchymal Fgf signals during later stages of tooth morphogenesis (Kwon et al., 2015). In the dental epithelium, *Runx2* and CCAAT/enhancer binding protein beta (*Cebpb*) act synergistically to prevent epithelial-mesenchymal transition (EMT) of odontogenic epithelial stem cells via snail family zinc finger2 (*Snai2*). Abrogating *Cebpb* and *Runx2* results in EMT and promotes *Sox2* expression and stemness of oral epithelial stem cells, leading to supernumerary teeth forming around the labial portion of the cervical loop in $Cebpb^{-/-}$;$Runx2^{+/-}$ mice (Saito et al., 2018). *Runx2* is clearly important for early tooth development, but its potential function in regulating MSCs in adult tooth homeostasis is unknown.

In this study, we characterized the Gli1+ cell population in the mouse incisor using single-cell RNA sequencing (scRNA-seq). We revealed that Gli1+ cells constitute a heterogeneous population and identified a subpopulation characterized by expression of *Runx2* in the proximal region of the adult incisor. These Runx2+ cells are located close to both MSCs and TACs and are thus strategically positioned to support the stem cell niche environment. Furthermore, insulin-like growth factor binding protein (Igfbp) 3 secreted by these Runx2+

cells activates insulin-like growth factor (IGF) 2 signaling to regulate TAC proliferation and differentiation. We demonstrated that this subpopulation of Runx2+/Gli1+ niche cells controls the rate of incisor growth in adult mice. This discovery improves our understanding of the stem cell niche microenvironment and has broad implications concerning the heterogeneity of Gli1+ cells and their roles in regulating tissue homeostasis.

RESULTS

Runx2 Is Expressed in a Subpopulation of Gli1+ Cells in the Proximal Region of the Incisor

MSCs in the mouse incisor have been reported to be labeled by heterogeneous markers (An et al., 2018b; Feng et al., 2011; Kaukua et al., 2014; Zhao et al., 2014). To elucidate the heterogeneity of the MSC population in the adult mouse incisor, we performed scRNA-seq analysis on incisors from 1-month-old wild-type mice (Figure 1A). Unbiased t-distributed stochastic neighbor embedding (t-SNE) showed *Gli1* expression in the dental mesenchyme, as well as the epithelium (Figure 1B). Gli1+ cells were selected and re-clustered through t-SNE analysis. Results showed that Gli1+ cells consisted of nine distinct clusters (Figure 1C). We validated and mapped the clusters based on the selected marker gene expression (Figure S1A). We analyzed specific genes in different clusters and identified that *Runx2* was highly expressed in a subpopulation located in the proximal region (Figure 1D). To validate the scRNA-seq analysis *in vivo*, we checked the expression pattern of Runx2 using immunofluorescence staining and confirmed that it is expressed in the proximal region of the incisor mesenchyme, mainly in the lateral portion close to the cervical loop (Figures 1E and 1F). Runx2 expression was also detected in the periodontal ligament and in some odontoblasts (Figure 1E). To visualize the relationship between Runx2+ cells and Gli1+ cells, we analyzed the colocalization of Runx2+ cells with Gli1+ cells using *Gli1-LacZ* mice. We found that Runx2+ cells overlapped with Gli1+ cells mainly in the region adjacent to the cervical loop (Figures 1G and 1H). To determine whether Runx2+ cells overlapped with TACs, we performed double staining of Runx2 and TAC marker Ki67, which revealed that Runx2+ cells and TACs were adjacent but mutually exclusive cell populations (Figures 1I and 1J). This expression of *Runx2* in Gli1+ cells suggested that it may play a critical role in the mesenchymal tissue homeostasis of the mouse incisor.

Loss of Runx2 in the Gli1+ Lineage Impairs the Incisor Growth Rate

Mouse incisors self-renew throughout the animal's life with the support of Gli1+ MSCs. Because *Runx2* is expressed in a subpopulation of Gli1+ cells, we tested whether *Runx2* is essential in regulating stem cell fate and therefore incisor homeostasis. We generated *Gli1-Cre^{ERT2};Runx2$^{fl/fl}$* mice in which *Runx2* was inactivated in the Gli1+ lineage after induction with tamoxifen at one month of age. Immunofluorescence staining confirmed that Runx2 was efficiently deleted from the incisor mesenchyme (Figure S1B). We observed that the incisors of these mice had decreased in length 1 month after deletion of *Runx2* (Figures 2A and 2B), which was confirmed by micro-computed tomography (micro-CT) (Figures 2C and 2D). Three months later, we noticed more significant shortening of incisors in *Runx2* mutant mice (Figures 2E–2I). To observe the incisor growth rate dynamically, we made a notch in the incisor enamel close to the junction with the gingiva one day after induction and measured the growth of the incisor as revealed by the movement of the notch 3 and 6 days

later. The notch movement was significantly slower in *Runx2* mutant mice after 6 days (Figure S2A). This is consistent with our finding that the ability to repair the incisor after clipping was compromised in *Runx2* mutant mice (Figure S2B).

These data indicate that loss of Runx2 affected tissue homeostasis and eventually retarded the growth rate of incisors in *Gli1-Cre^{ERT2};Runx2$^{fl/fl}$* mice. Histological analysis revealed abnormal dentin formation and disorganized epithelium near the cervical loop (Figures 2J–2M) one month after induction. The expression of odontoblast differentiation marker dentin sialophosphoprotein (*Dspp*) was closer to the proximal end of the incisor in the *Runx2* mutants compared with control mice (Figures 2N–2Q), suggesting that Runx2 plays an essential role in regulating odontoblast differentiation.

Because Gli1+ cells contribute to the periodontal ligament in the adult mouse incisor (Figures 4Ba and 4Bc), Runx2 was also deleted from the periodontal ligament in *Gli1-Cre^{ERT2};Runx2$^{fl/fl}$* mice. We found defects in the periodontal ligament and alveolar bone in *Gli1-Cre^{ERT2};Runx2$^{fl/fl}$* mice (Figure S2C). These data indicated that Runx2+ cells also play an important role in the homeostasis of the periodontium.

It has been reported that Gli1+ cells contribute to both mesenchymal and epithelial cell lineages (Seidel et al., 2010; Zhao et al., 2014) and that Runx2 is expressed in mature ameloblasts (Figure S3B). To rule out the possibility that the changes we observed in the mesenchyme after deletion of Runx2 were secondary to changes in the epithelium, we generated *Sox2-Cre^{ERT2};Runx2$^{fl/fl}$* mice with inducible deletion of *Runx2* in the Sox2+ cells, which exclusively contribute to the epithelium (Figure S3A) (Juuri et al., 2012). We induced these mice with tamoxifen at one month of age. Four weeks after induction, Runx2 was lost only in the epithelium in *Sox2-Cre^{ERT2};Runx2$^{fl/fl}$* mice (Figure S3D). Dentin formation was unaffected in the incisors, based on micro-CT analysis and H&E staining (Figures S3F–S3J). These data suggested that loss of Runx2 in the ameloblasts had no effect on the proximal dental mesenchyme.

Runx2+ Cells Are Niche Cells that Maintain Tissue Homeostasis in the Mouse Incisor

Because Runx2+ cells colocalized with Gli1+ cells, we sought to determine whether Runx2+/Gli1+ cells are a subpopulation of MSCs. We generated *Runx2-rtTA;tetO-Cre;tdTomato* mice to perform lineage tracing of Runx2+ cells in the adult mouse incisor. One week after induction at one month of age, Runx2+ cells were present in the proximal region of the mesenchyme (Figures 3A and 3B). Analysis at one and three months after induction showed that Runx2+ cells remained in the proximal region of the incisor and did not differentiate into odontoblasts or dental pulp cells, suggesting that Runx2+ cells do not contribute to the dental mesenchyme during incisor growth (Figures 3C–3F). To assess whether Runx2+ cells contribute to injury repair, we clipped one incisor to approximately half of its length (Figure 3H). Three days after clipping, the injured side was almost repaired such that its length was comparable to that of the uninjured contralateral incisor (Figure 3K). However, Runx2+ cells still did not move away from the proximal region of the incisor or differentiate into odontoblasts during injury repair (Figures 3I and 3L). We also quantified the percentage of Runx2+ cells at different stages. The statistical analysis showed that there

was no significant difference in the percentage of Runx2+ cells during growth or injury repair (Figures 3G and 3N).

To evaluate the relationship between Runx2+ cells and label-retaining cells (LRCs), which are considered a population of quiescent stem cells, we injected EdU daily into pups for 4 weeks beginning at postnatal day 5 and traced 5-Ethynyl-2'-deoxyuridine (EdU) incorporation for another 8 weeks. The EdU staining showed that LRCs did not overlap with Runx2+ cells (Figure S4). Collectively, based on these data, we concluded that Runx2+/Gli1+ cells are not MSCs. Nevertheless, they reside in the MSC niche and play an important role in regulating growth and tissue homeostasis of adult mouse incisors.

Runx2+ Cells Maintain the Incisor MSC Niche by Regulating TAC Proliferation and Differentiation

Although Runx2+/Gli1+ cells are not MSCs, *Gli1-Cre*^{ERT2}; *Runx2*$^{fl/fl}$ mice showed a reduced incisor growth rate. To elucidate how Runx2+ cells control growth and tissue homeostasis via regulating the incisor MSC niche, we first quantified the Gli1+ MSC population in *Gli1-Cre*^{ERT2};*Runx2*$^{fl/fl}$;*Gli1-LacZ* mice. The number of Gli1+ cells in *Gli1-Cre*^{ERT2};*Runx2*$^{fl/fl}$;*Gli1-LacZ* mice remained the same as in *Gli1-LacZ* mice one week after induction (Figures 4Aa and 4Ac) but significantly decreased two weeks after induction (Figures 4Ae and 4Ag). To investigate the effect of *Runx2* loss on the differentiation of Gli1+ MSCs, we assessed the contribution of MSCs to their progeny, comparing *Gli1-Cre*^{ERT2};*tdTomato* and *Gli1-Cre*^{ERT2};*Runx2*$^{fl/fl}$;*tdTomato* mice. We measured the length of dental pulp that was positive for the tdTomato signal, representing the Gli1+ cells' progeny in the incisor; we then computed this length as a percentage of the length of the whole dental pulp (Figure 4Be). One week after induction, the percentage of Gli1+ cells' progeny measured in this manner was unchanged (Figures 4Ba, 4Bb, and 4Bf), but it significantly decreased 2 weeks after induction in *Runx2* mutant mice (Figures 4Bc, 4Bd, and 4Bg), suggesting that the differentiation rate had slowed.

We also checked the number and differentiation of TACs. The number of TACs decreased significantly one week after induction in *Gli1-Cre*^{ERT2};*Runx2*$^{fl/fl}$ mice, as detected by Ki67 immunofluorescence staining (Figures 4Ca, 4Cc, and 4Ci); there was no concomitant increase in apoptosis detected by TUNEL assay (Figure S5A).

Next, we assessed whether there was a change in the TAC differentiation rate in *Runx2* mutant incisors. We first identified that the number of TACs was comparable in *Runx2* mutant and control mice 5 days after induction (Figure S5B). Then, we injected EdU 5 days after induction and assessed the TAC differentiation rate upon euthanizing the mice 48 h later. Because TACs retain EdU during differentiation in this short time frame, the length of overlap between *Dspp*+ odontoblasts and EdU+ cells reflected the number of TACs that underwent odontogenic differentiation in this period. Strikingly, there were fewer double-positive cells in *Runx2* mutant incisors compared with the controls (Figures 4Cf, 4Ch, and 4Cj), showing that differentiation of TACs was perturbed in *Runx2* mutant mice one week after induction. Clearly, loss of *Runx2* in the Gli1+ lineage first led to compromised TAC proliferation and differentiation and then affected the MSC population, which suggests that

Runx2+ cells maintain the incisor MSC niche by regulating TAC proliferation and differentiation.

Runx2-Regulated IGF-2 Signaling Is Crucial for Incisor Tissue Homeostasis

To identify downstream components of the molecular mechanism by which Runx2 regulates the MSC niche, we analyzed gene expression in the proximal region of the incisor by performing RNA-seq on adult *Runx2*$^{fl/fl}$ and *Gli1-Cre*^{ERT2};*Runx2*$^{fl/fl}$ mice one week after induction. Hierarchical clustering showed that gene expression profiles of *Runx2* mutant and control mice were well separated (Figure 5A). Five hundred and eleven differentially expressed genes were identified (>2-fold, $p < 0.05$), of which 299 were upregulated and 212 were downregulated (Figure 5B). Analysis of these genes using Ingenuity Pathways Analysis (IPA, QIAGEN) revealed that several signaling pathways related to cell-cycle regulation were highly involved, such as p53 signaling, cyclins and cell-cycle regulation, IGF signaling, and Wnt/β-catenin signaling (Figure 5C). We focused on IGF signaling, which is known to play an important role in the MSC niche (Youssef et al., 2017; Ziegler et al., 2019). Specifically, we confirmed that Igf2 protein was downregulated in the Runx2+ and TAC regions of *Runx2* mutant incisors (Figure 5Dc) compared with controls (Figure 5Da). The IGF1 receptor (Igf1r) was detected in the TAC region by RNAscope in both control and *Runx2* mutant mice (Figure S6A). Igf1r could be phosphorylated in control mice (Figure 5De) but failed to be phosphorylated in mesenchymal TACs in *Runx2* mutant mice (Figure 5Dg). The expression of phosphorylated insulin receptor substrate 1 (p-Irs1) was also decreased in *Runx2* mutant mice (Figures 5Di and 5Dk). Phosphorylated Akt (p-Akt), a downstream target of IGF signaling, was downregulated (Figures 5Dm and 5Do). These results were confirmed by western blot (Figure 5E).

Igfbp3 Secreted by Runx2+ Cells Is Indispensable for Maintaining IGF-2 Signaling

To explore how Runx2+ cells regulate *Igf2*, we first checked the mRNA expression pattern of *Igf2*. *Igf2* was highly expressed in the MSC region in both control and *Runx2* mutant incisors (Figures S6Ba and S6Bc). Analysis following real-time PCR showed that there was no significant difference in *Igf2* mRNA expression levels between control and *Runx2* mutant groups (Figure S6Be). The activity of the IGF ligands is regulated by a family of six IGFBPs in vertebrates. Therefore, we performed RNAscope to visualize the mRNA expression of each of the IGFBPs (Figure S6C). We then narrowed our focus to *Igfbp3*, which was specifically downregulated in Runx2+ cell region following the loss of *Runx2*. We detected the expression pattern of *Igfbp3* at the mRNA level using RNAscope. In control mice, Runx2 proteins and *Igfbp3* mRNA were colocalized in the same cells (Figure 5Fa). After deleting *Runx2*, the expression of *Igfbp3* was undetectable specifically in the apical region, where Runx2+ cells would have been located (Figure 5Fc). We confirmed that the expression level of *Igfbp3* was downregulated in the *Runx2* mutant incisor using real-time PCR (Figure 5Fe). However, the expression pattern of *Igfbp3* in the periodontal ligament remained comparable between *Runx2* mutant incisors (Figure 5Fa) and control incisors (Figure 5Fc), suggesting that Runx2 regulates the periodontium independently, through other mechanisms. To test the function of Igfbp3 in the mouse incisor, we cultured MSCs from control and *Runx2* mutant incisors with serum-free media with or without Igfbp3. The

concentration of Igf2 in the culture supernatant, detected using ELISA, was rescued in the *Runx2* mutant group with Igfbp3 (Figure 5G).

To determine whether Runx2 can directly regulate *Igfbp3*, we performed Assay for Transposase-Accessible Chromatin using sequencing (ATAC-seq) to assess genome-wide chromatin accessibility. We found that there is a Runx2 binding motif located at the promoter of *Igfbp3* (Figure 5H), which is consistent with a previously discovered Runx2 motif associated with genes regulating osteoblast differentiation (Wu et al., 2014). These motifs share a 5′-TGTGGT core sequence with the Runx2 binding consensus sequence (Portales-Casamar et al., 2010). Chromatin immunoprecipitation (ChIP) coupled with qPCR provided direct evidence that Runx2 can bind to *Igfbp3* (Figure 5I). These results demonstrate that Igfbp3 secreted by Runx2+ cells is indispensable for IGF-2 signaling in the mouse incisor.

IGF-2 Rescues Proliferation and Odontogenic Differentiation of MSCs from *Gli1-Cre^{ERT2};Runx2$^{fl/fl}$* Mice *In Vitro*

Next, we tested the function of Igf2 in regulating MSC proliferation and odontogenic differentiation *in vitro*. The number of colonies formed by MSCs from *Gli1-Cre^{ERT2};Runx2$^{fl/fl}$* mice (Figure 6C) decreased significantly compared with those formed by MSCs from *Runx2$^{fl/fl}$* mice (Figure 6A). Adding Igf2 protein to the culture media rescued the colony formation in the *Runx2* mutant group (Figure 6D) but had little effect on the control group (Figures 6B and 6E). We then induced MSCs from *Runx2* mutant and control incisors to undergo odontogenic differentiation. Seven days after odontogenic induction, we checked the expression of *Dspp* using RNAscope *in situ* hybridization. The expression of *Dspp* in mutants (Figure 6H) was downregulated compared with controls (Figure 6F). Adding Igf2 protein to the odontogenic induction medium upregulated the expression of *Dspp* in *Runx2* mutant MSCs (Figure 6I), but not the control group (Figure 6G). qPCR confirmed that the gene expression level of *Dspp* significantly increased in the *Runx2* mutant group with Igf2 treatment (Figure 6J). We checked the calcium deposition during odontogenic differentiation by Alizarin red staining (Kaukua et al., 2014; Li et al., 2018). MSCs from the *Runx2* mutant (Figure 6M) deposited less calcium than those from the control (Figure 6K) after 3 weeks of odontogenic induction. Adding Igf2 to the odontogenic induction medium enhanced the deposited calcium significantly in the *Runx2* mutant group (Figure 6N), but not in the control group (Figures 6L and 6O). Western blotting confirmed that IGF signaling was activated in the *Runx2* mutant group with Igf2, but not in the *Runx2* mutant group without Igf2 (Figure 6P). These results suggest that Igf2 could rescue proliferation and odontogenic differentiation of MSCs in *Runx2* mutant mice *in vitro*.

DISCUSSION

Genetic cell lineage tracing has identified that the MSCs in the adult mouse incisor are a population labeled by *Gli1* and maintained by Shh secreted from a neurovascular bundle niche (Zhao et al., 2014). These MSCs are crucial in supporting the continuous growth of the rodent incisor throughout the animal's life. In this study, we have uncovered previously unknown heterogeneity of Gli1+ cells in the adult mouse incisor. We identified an

unexpected subpopulation of Gli1+ cells strategically located close to MSCs and TACs in the proximal region of the adult mouse incisor. This subpopulation is characterized by expression of *Runx2*. The Runx2+ cells are niche cells that secrete Igfbp3 and activate IGF-2 signaling to regulate TAC proliferation and differentiation to control the incisor growth rate and maintain tissue homeostasis.

Specialized niches support adult stem cells, which reside within them in a quiescent state (van Velthoven and Rando, 2019). In many ectodermally derived organs, such as in lung epithelium (Lee et al., 2017), intestinal epithelium (Ganz, 2000; Sato et al., 2011), and hair follicle (Gonzales and Fuchs, 2017; Yang et al., 2017), the specialized stem cell niches have been well characterized. These studies took advantage of the well-defined anatomical structures in which ectodermal stem cells and their niche are present. Stem cells may act upon or generate their niche to control tissue homeostasis (Clevers et al., 2014). Furthermore, niche cells and factors they secrete play critical roles in regulating stem cells in tissue homeostasis and diseases. For example, niche cells produce signals to induce quiescent neural stem cells to activate and renew themselves (Song et al., 2012). In lung adenocarcinomas, niche cells produce the Wnt ligand, which regulates stem cells and affects tumor progression (Tammela et al., 2017). In contrast to stem cells in the ectoderm, MSCs and their niche environments are still not well understood.

The adult mouse incisor offers a well-defined model to investigate the MSCs and their interaction with neighboring TACs (Shi et al., 2019; Zhao et al., 2014). For example, a recent study has shown that polycomb Ring1 regulates TAC proliferation by inhibiting Cdkn2a and regulating the activity of Wnt/β-catenin signaling. Depletion of Ring1b in TACs causes specific apoptosis of the stem cells, suggesting that TACs can provide positive feedback to MSCs (An et al., 2018a). To date, however, the niche cell populations for MSCs have yet to be defined, and it is unknown how these niche cells may operate. We have identified a previously unknown population of *Runx2*+/*Gli1*+ cells that act as niche cells to regulate TAC proliferation and differentiation and can control the growth rate of the adult mouse incisor. These results provide new insights into the MSC niche in the adult mouse incisor and its functional significance in regulating tissue homeostasis in this organ.

The stem cell niche involves cell-cell interactions that regulate the fate of MSCs. We discovered that loss of *Runx2* in niche cells led to compromised TAC proliferation and differentiation one week after induction. However, we also noted abnormal dentin formation and increased thickness of dentin one month after induction. The function of Runx2 is cell type specific and depends upon the stage of cell differentiation. For example, Runx2 activates *Dspp* expression in preodontoblasts but represses this gene later in odontoblast differentiation (Chen et al., 2005; Miyazaki et al., 2008). Here we found that deleting Runx2 in Gli1+ cells first affected TAC proliferation and differentiation. Notch movement and injury repair assays also showed that odontogenesis was compromised. These results suggest that Runx2 regulates odontogenesis by promoting odontogenic lineage commitment early in the differentiation process. At a later stage, we observed increased dentin thickness. This was likely because of loss of Runx2 in the progeny of Gli1+ cells, such as odontoblasts. In odontoblasts, Runx2 inhibits *Dspp* expression (Chen et al., 2005). Loss of Runx2 in odontoblasts leads to premature *Dspp* expression and thicker dentin. Another probable

reason for the increased dentin thickness is that the migration of Gli1+ cell progeny is slower in *Runx2* mutant incisors, which could also cause increased accumulation of dentin matrix.

We found that Runx2 regulates IGF signaling to control odontoblast differentiation and the growth rate of the adult mouse incisor. The IGF signaling axis is critical in regulating stem cell self-renewal and differentiation. Upon binding the IGF ligands IGF-1 and IGF-2, Igf1r is activated through autophosphorylation and in turn activates its downstream targets through the phosphatidylinositol 3-kinase/protein kinase B (PI3K/AKT) or Ras/mitogen-activated protein kinase (MAPK) signaling pathway (Hakuno and Takahashi, 2018; Youssef et al., 2017). It has been shown that IGF-2 is required to maintain human embryonic stem cell self-renewal and pluripotency via Igf1r signaling (Bendall et al., 2007). During bone remodeling, IGF-1 is released from the bone matrix, where it recruits MSCs to undergo osteoblastic differentiation by activating mammalian target of rapamycin (mTOR); IGFBP3 facilitates this process by inducing IGF-1 to deposit in the bone matrix (Xian et al., 2012). In human dental pulp MSCs (hDSCs), Igf1r is correlated with retaining pluripotency and self-renewal capacity and can induce neurite regeneration and neuroplasticity after hDSC transplantation in a stroke model (Lee et al., 2016).

In this study, we have uncovered a Runx2-IGF signaling network in the MSC niche of the adult mouse incisor. *Igf2* mRNA was barely detected in the TAC region, but Igf2 protein could be detected in the TAC region in control mice, suggesting that Igf2 may regulate TAC proliferation and differentiation in a paracrine manner. Loss of Runx2 led to downregulation of Igf2 and failure of Igf1r phosphorylation in the adult mouse incisor. Moreover, the IGF downstream targets p-Irs1 and p-Akt were significantly downregulated in *Runx2* mutant mice. Significantly, exogenous Igf2 could rescue MSC proliferation and odontoblast differentiation defects in incisors of adult *Runx2* mutant mice, whereas Igf2 did not enhance proliferation and differentiation of MSCs from control ($Runx2^{fl/fl}$) incisors. These data suggest that Igf2 is necessary and sufficient to sustain a Runx2-Igf signaling cascade within the MSC niche.

It is well known that the IGF ligands in the circulation and throughout the extracellular space bind with high affinity to IGFBPs. The IGFBPs have several functions, which include prolonging the half-lives of IGFs, localizing IGFs to particular types of cells, and modulating interactions between IGFs and their receptors (Clemmons, 1993, 2016; Firth and Baxter, 2002; Jones and Clemmons, 1995). Our study has shown that Igfbp3 is specifically required for Igf2 signaling as part of the MSC niche signaling network in the adult mouse incisor. IGFBP3 is the most abundant member of the IGFBP family (Allard and Duan, 2018; Clemmons, 2018). In the extracellular environment, most IGFs bind with IGFBP3 to protect ligands from degradation and facilitate delivery to specific tissues (Duan and Xu, 2005; Ranke, 2015). Through ATAC-seq and ChIP-qPCR, we have shown that Runx2 directly regulates *Igfbp3* gene expression. Collectively, these data suggest that Igfbp3 secreted by Runx2+ cells is essential for IGF2 signaling in regulating tissue homeostasis in the adult mouse incisor.

In conclusion, we have uncovered heterogeneity among Gli1+ cells in the adult mouse incisor that reflects complex functions of MSCs in maintaining tissue homeostasis and repair. We have identified a previously unknown population of Runx2+ cells in the MSC region that are niche cells, but not MSCs. We showed that these Runx2+ niche cells regulate TAC proliferation and differentiation via IGF signaling. Igfbp3 secreted by Runx2+ cells is critical for IGF signaling in the mouse incisor. Our study provides insights into the mechanisms of how stem cell niches work as a local ecosystem to maintain tissue homeostasis, which may also have important implications for tissue regeneration.

STAR★METHODS

Detailed methods are provided in the online version of this paper and include the following:

RESOURCE AVAILABILITY

Lead Contact—Further information and requests for resources and reagents should be directed to and will be fulfilled by the Lead Contact, Yang Chai (ychai@usc.edu).

Materials Availability—All unique/stable reagents generated in this study are available from the Lead Contact without restriction.

Data and Code Availability—The scRNA-seq data, bulk RNA-seq data and ATAC-seq data of mouse incisors in this publication have been deposited in NCBI's Gene Expression Omnibus and are accessible through GEO Series accession number GSE154158 (https://www.ncbi.nlm.nih.gov/geo/query/acc.cgi?acc=GSE154158).

EXPERIMENTAL MODEL AND SUBJECT DETAILS

Animals—Mice used in this study included *Gli1-Cre*^{ERT2} knock-in (JAX#007913), *ROSA26*$^{loxp\text{-}STOP\text{-}loxp\text{-}tdTomato}$ conditional reporter (JAX#007905, (Madisen et al., 2010), *Gli1-LacZ* heterozygotes (JAX#008211, (Bai et al., 2002), *Sox2-Cre*^{ERT2} knock-in (JAX#017593, (Li et al., 2015), *Runx2-rtTA* (gift from Fanxin Long, Washington University School of Medicine; (Chen et al., 2014), *tetO-Cre* (JAX#006234), *C57BL/6J* (JAX#000664), and *Runx2*$^{flox/flox}$ (gift from Dr. Takeshi Takarada, Okayama University, Japan; (Takarada et al., 2013). Mice were housed in pathogen-free conditions and analyzed in a mixed background. All mice were used for analysis without consideration of sex. All mice were induced at one month of age and euthanized at specific stage as described in figure legend. Genotyping was performed from ear biopsies, which were lysed in DirectPCR tail solution (Viagen 102 T) through incubation at 55°C overnight followed by 85°C heat inactivation for 30 min. PCR-based genotyping (GoTaq Green MasterMix, Promega, and C1000Touch Cycler, Bio-rad) was conducted to identify the mouse lines. All mouse experiments were approved by the Institutional Animal Care and Use Committee at the University of Southern California.

METHOD DETAILS

Tamoxifen and doxycycline administration—Tamoxifen (Sigma, T5648) was dissolved in corn oil (Sigma, C8267) at 20 mg/ml and injected intraperitoneally at a dosage

of 1.5mg/10 g body weight daily for 3 consecutive days. Doxycycline rodent diet (ENVIGO, TD.08541) was administered every day.

scRNA Sequencing—Four-week-old wild-type *C57BL/6J* mice were used for single-cell transcriptomics experiments. Mandibles were carefully dissected under a stereomicroscope. The surrounding jaw bones were removed by scalpel and the proximal region was then severed. Dental pulp with dental epithelium was isolated, cut into pieces, collected in cold PBS, and digested with 2mg/ml collagenase type I (Worthington, LS004194) dissolved in α-MEM (GIBCO, 12571–048) for 30 min at 37°C. After incubation, the suspension was homogenized by pipetting and digestion was terminated by adding 10% FBS. The digested tissues were centrifuged at 300 g for 5 min and resuspended in 10% FBS. Twenty thousand cells were loaded into the 10X Chromium system with targeted cell recovery of 10,000 cells to be barcoded for scRNA-seq using a Single Cell 3′ Library Kit v3. Sequencing was performed on the Illumina Novaseq System. About 9,318 cells (~63,000 reads per cells) were successfully barcoded and their transcriptomes sequenced. Raw read counts were analyzed using the Seurat R package (Satija et al., 2015).

EdU incorporation and staining—For TAC differentiation, EdU (25 μg/g body weight) was intraperitoneally (IP) injected once at 5 days after induction of *Gli1-Cre*^{ERT2};*Runx2*$^{fl/fl}$ mice and *Runx2*$^{fl/fl}$ mice. Mice were euthanized and samples were collected 48 hours after Edu injection. For label-retaining cell assay, EdU was IP injected into pups daily beginning at postnatal day 5 for 4 weeks and washed out for another 8 weeks. After euthanasia, the mandible was collected, fixed, and decalcified, followed by cryo-sectioning. Edu was detected using a Click-iT Plus EdU Cell Proliferation Kit (Invitrogen, *C10637*)

MicroCT analysis—MicroCT analysis was performed on a SCANCO μCT50 (Scanco V1.28) device at the University of Southern California Molecular Imaging Center. Images were acquired at a resolution of 10 μm with the X-ray source at 90 kVp and 78 μA. Three-dimensional (3D) reconstruction was completed with AVIZO 7.1 (Visualization Sciences Group).

Immunofluorescence staining—For immunofluorescence analysis, the dissected mouse mandibles were fixed in 4% paraformaldehyde (PFA) overnight, and then decalcified with 10% EDTA for four weeks.

Then, the tissues were dehydrated in 15% sucrose/PBS solution for two hours, then in 30% sucrose/PBS for two hours, and 30% sucrose/OCT (Sakura, Tissue-Tek, 4583) at 4°C overnight followed by embedding in OCT. Sagittal cryosections 8 μm thick were used for immunofluorescence staining following standard protocols. The primary antibodies are listed in Table S1. Alexa Fluor 488 and Alexa Fluor 568 (1:200, Invitrogen) were used as secondary antibodies. DAPI (Invitrogen, 62248) was used for nuclear staining. All images were captured using a Keyence microscope (Carl Zeiss). For p-Igf1r, p-Irs1, p-Akt and Igf2, Alexa Fluor 488/594 Tyramide SuperBoost kits (Invitrogen, B40922/40925) were used.

TUNEL assays—Apoptosis was detected using a TUNEL assay (Click-iT Plus TUNEL Assay for *In Situ* Apoptosis Detection, Thermo Fisher, C10617) according to the recommended protocol.

RNAscope *in situ* hybridization (ISH)—Cryosections were used for ISH. RNAscope® Multiplex Fluorescent v2 (Advanced Cell Diagnostics, 323110) was used following the protocols of the manufacturer. The signal was detected by TSA Plus Cyanine 3 (System Perkin Elmer, NEL744001KT). All probes used in this study were designed and synthesized by Advanced Cell Diagnostics. Probe details are included in the Key Resources Table.

Quantitative Real-time PCR—The RNeasy Plus Micro Kit (QIAGEN, 74004) was used for extraction of total RNA from incisor dental mesenchyme of *Runx2*$^{fl/fl}$ and *Gli1-Cre*^{ERT2};*Runx2*$^{fl/fl}$ mice one week after tamoxifen induction at one month of age. cDNA was synthesized using an iScriptcDNA Synthesis Kit (Bio-Rad, 1708890). Real-time quantitative PCR was then performed using Sso Fast Eva Green® Supermix (Bio-Rad, 1725201) and a CFX 96 Real-time System (Bio-Rad). *Gapdh* expression was used to normalize gene expression. All primers are listed in Table S2.

Incisor injury and notch movement experiments—The mice were anesthetized with isoflurane. The incisor was clipped by removing the erupted part aligned with the gingival papilla. To assess notch movement, a notch was made above the gumline using a carbide bur (Brasseler USA®, 018554U0). Measurements were taken using a digital caliper (VWR® Digital Calipers,62379–531).

ImageJ image analysis—ImageJ was used to calculate the percentage of positive immunofluorescence signals in the TAC and MSC regions. The length of incisor, the amount of tdTomato signal, and overlap between EdU signal and *Dspp* were measured in ImageJ as well.

Colony formation assay—MSCs were harvested as previously described (Zhao et al., 2014). In brief, the proximal region of lower incisor mesenchyme was obtained from 1-month old *Runx2*$^{fl/fl}$ and *Gli1-Cre*^{ERT2};*Runx2*$^{fl/fl}$ mice 5 days after induction. The epithelium was dissected and removed with fine forceps. The pulp tissue was cut into pieces and digested with solution containing 2mg/ml collagenase type I (Worthington, LS004194) in PBS for 30 min at 37°C. A single-cell suspension was harvested through 70 μm strainer (Falcon, 352350) and seeded at 2×10^4/well into 24-well culture plate with growth media (α-MEM [Thermo Fisher Scientific, 12571–048] supplemented with 10% fetal bovine serum [FBS],100 U·mL^{-1} penicillin, and 100 U·mL^{-1} streptomycin) in 5% CO_2 at 37°C. Initial cultures were left undisturbed for 2 days to allow cell adhesion. Then the growth media was changed every other day supplemented with or without 100ng/ml mouse recombinant Igf2 (Sigma-Aldrich, 18904) according different groups (showed in Figure 6). After 7 days, the culture plates were stained with 0.1% toluidine blue together with 2% paraformaldehyde solution. Colonies containing more than 50 cells were counted as a single colony cluster.

MSC odontogenic differentiation—The dental mesenchyme was obtained from 1-month old *Runx2*$^{fl/fl}$ and *Gli1-Cre*^{ERT2};*Runx2*$^{fl/fl}$ mice 5 days after induction as described above. The pulp tissue was cut into pieces and incubated with growth media in 6-well plate. The culture media was left to rest for 4 days to allow tissue adhesion and cell migration. Then the culture media was changed every other day.

2×10^5 MSCs were plated in a 4-well chamber slide (PEZGS0416, Millipore) or 24-well plate (Nest, 702011) and induced in odontogenic differentiation media containing 1% FBS, β-glycerophosphate (β-GP) (5mM), ascorbic acid (50μg/ml), and dexamethasone (DEX) (10nM). 100 ng/ml mouse recombinant Igf2 was added to odontogenic induce media according different groups (showed in Figures 6F–6I). For *Dspp* RNAscope *in situ* hybridization, cells cultured in a 4-well chamber slide were harvested 7 days after induction and the standard protocols of the manufacturer were then followed. To detect mineralized nodules, cells were induced for 21 days, fixed with 4% paraformaldehyde, and stained with 2% Alizarin red S (pH4.2) (ACROS Organics, 400480250). Alizarin red-S contents were extracted with 10% cetylpyridinium chloride in distilled water and measured at 590 nm on SpectraMax iD3 (Molecular Devices, LLC., San Jose, USA).

ELISA—The dental MSCs from *Runx2*$^{fl/fl}$ and *Gli1-Cre*^{ERT2};*Runx2*$^{fl/fl}$ mice was harvested as described above. 5×10^4 MSCs were seeded on 48-well plate (Nest,748011) with growth media. After 80% confluency, the culture plate was washed with Phosphate-buffered saline (PBS) for three times and then added 200 μL serum-free media, i.e., α-MEM with or without 50nM mouse recombinant Igfbp3 protein (R&D Systems, 775-B3). The supernatant was harvested at different time point (showed in Figure 5I) and stored at −20°C. The concentration of Igf2 was detected by Mouse/Rat/Porcine/Canine IGF-II/IGF2 Quantikine ELISA Kit (R&D Systems, MG200). The assay procedure followed the manufacture's protocol.

Western blot—For western blots, the proximal region of incisor mesenchyme and cultured cells were lysed by RIPA buffer (Cell Signaling, 9806) supplemented with Protease inhibitor (ThermoFisher Scientific, A32959) for 30 min on ice. Protein extracts were loaded in 4%–15% precast polyacrylamide gel (Bio-Rad,456–1084), transferred to 0.45 μm PVDF membrane, blocked with 5% milk (Bio-Rad,170–6404) for 1h, and incubated with primary antibody (Table S1) at 4°C overnight. After incubation with HRP-conjugated secondary antibody for 1 h at room temperature, signals were detected using Azure 300 (Azure biosystems) and images were taken with cSeries Capture Software.

RNA sequencing—Incisor samples taken one week after induction of one-month-old *Gli1-Cre*^{ERT2};*Runx2*$^{fl/fl}$ and *Runx2*$^{fl/fl}$ mice were dissected. The proximal region was collected for RNA isolation with an RNeasy Micro Kit (QIAGEN). The quality of RNA samples was evaluated using an Agilent 2100 Bioanalyzer and all samples used for sequencing had RNA integrity (RIN) numbers > 9.0. cDNA library preparation and sequencing were performed by DNA Link, Inc. Single-end reads with 75 cycles were performed on NextSeq500 for three pairs of samples. Raw reads were trimmed, aligned using STAR (version 2.6.1d) with the mm10 genome, and normalized using Upper quartile.

Differential expression was calculated by selecting transcripts that had significant changes of $p < 0.05$.

ATAC-sequencing—The proximal dental mesenchyme of mouse incisor was dissected from 4-week-old wild-type *C57BL/6J* mice. A cell suspension was prepared as described above for scRNA sequencing. Five thousand cells were obtained, spun down, and washed once with cold PBS. Then the cells were resuspended in cold lysis buffer. The transposition reaction, purification and PCR application followed a previously described protocol (Buenrostro et al., 2015). Transposed DNA libraries were sequenced on NextSeq500 High-Output 150 cycles (75PE). ATAC-seq reads were aligned to the UCSC mm10 reference genome with BWA-MEM (Li, 2013). ATAC-seq peaks were called through MACS2 (Zhang et al., 2008). Peaks were annotated and known transcription factor binding motifs were further analyzed in the ATAC-seq peaks by HOMER (Heinz et al., 2010).

ChIP-qPCR—The proximal mesenchymal tissue was dissected from 4-week-old wild-type *C57BL/6J* mice. For each replicate, 60–80mg tissue was combined as one sample. The sample was prepared following the manufacturer's protocol (Chromatrap,500191). Briefly, The tissue was cut into small pieces, fixed with 1% formaldehyde at room temperature for 15 minutes and then quenched by 0.65 M glycine solution. The sample was washed twice with PBS, resuspended with Hypotonic Buffer and incubate at 4°C for 10 minutes to get the pellet (nuclei). The pellet was resuspended in Digestion Buffer and chromatin was sheared to 100–500 bp fragments using Shearing Cocktail. 10 μg chromatin with Runx2 antibody (CST12556, 1:50) or Immunoglobulin G negative control (2ug) was added to Column Conditioning Buffer and made up to the final volume of 1000 μl. the immunoprecipitation (IP) slurry was then mixed well and incubated on an end to end rotor for 1 hour at 4°C. An equivalent amount of chromatin was set aside as an input. The IP slurry was loaded and flowed completely through the Chromatrap® spin column at room temperature. The column was washed three times with Wash Buffer and then the chromatin was eluted using a specially formulated ChIP-seq elution buffer. The chromatin sample was further incubated at 65°C overnight to reverse cross-linking, along with the untreated input. After treatment with proteinase K, DNA was purified with Chromatrap® DNA purification column. ChIP eluates, negative control and input were assayed by real-time q-PCR in a 20 μl reaction with the following: 1 μl of each primer (Table S2), 10 μl Eva Green® Supermix (Bio-Rad) using a CFX 96 real-time System (Bio-Rad). The primers were designed through amplifying Runx2-binding motifs in the *Igfbp3* promoter region (Table S2).

QUANTIFICATION AND STATISTICAL ANALYSIS

Statistical analysis was performed using GraphPad Prism. Paired Student's t tests and one-way analysis of variance (one-way ANOVA) were used to assess significance. Statistical data are presented as mean ± SEM $p < 0.05$ was considered statistically significant.

Supplementary Material

Refer to Web version on PubMed Central for supplementary material.

ACKNOWLEDGMENTS

We thank Dr. Bridget Samuels for critical reading of the manuscript. We thank USC Libraries Bioinformatics Service for assisting with data analysis. The bioinformatics software and computing resources used in the analysis are funded by the USC Office of Research and the USC Libraries. This study was supported by the National Institute of Dental and Craniofacial Research, National Institutes of Health (R01 DE025221, U01 DE028729, and R01 DE022503).

REFERENCES

Allard JB, and Duan C (2018). IGF-Binding Proteins: Why Do They Exist and Why Are There So Many? Front. Endocrinol. (Lausanne) 9, 117. [PubMed: 29686648]

An Z, Akily B, Sabalic M, Zong G, Chai Y, and Sharpe PT (2018a). Regulation of Mesenchymal Stem to Transit-Amplifying Cell Transition in the Continuously Growing Mouse Incisor. Cell Rep. 23, 3102–3111. [PubMed: 29874594]

An Z, Sabalic M, Bloomquist RF, Fowler TE, Streelman T, and Sharpe PT (2018b). A quiescent cell population replenishes mesenchymal stem cells to drive accelerated growth in mouse incisors. Nat. Commun 9, 378. [PubMed: 29371677]

Bai CB, Auerbach W, Lee JS, Stephen D, and Joyner AL (2002). Gli2, but not Gli1, is required for initial Shh signaling and ectopic activation of the Shh pathway. Development 129, 4753–4761. [PubMed: 12361967]

Bendall SC, Stewart MH, Menendez P, George D, Vijayaragavan K, Werbowetski-Ogilvie T, Ramos-Mejia V, Rouleau A, Yang J, Bossé M, et al. (2007). IGF and FGF cooperatively establish the regulatory stem cell niche of pluripotent human cells in vitro. Nature 448, 1015–1021. [PubMed: 17625568]

Blanpain C, and Fuchs E (2014). Stem cell plasticity. Plasticity of epithelial stem cells in tissue regeneration. Science 344, 1242281. [PubMed: 24926024]

Buenrostro JD, Wu B, Chang HY, and Greenleaf WJ (2015). ATAC-seq: A Method for Assaying Chromatin Accessibility Genome-Wide. Curr. Protoc. Mol. Biol 109, 21.29.21–21.29.29.

Chacón-Martínez CA, Koester J, and Wickström SA (2018). Signaling in the stem cell niche: regulating cell fate, function and plasticity. Development 145, dev165399. [PubMed: 30068689]

Chen S, Rani S, Wu Y, Unterbrink A, Gu TT, Gluhak-Heinrich J, Chuang HH, and Macdougall M (2005). Differential regulation of dentin sialophosphoprotein expression by Runx2 during odontoblast cytodifferentiation. J. Biol. Chem 280, 29717–29727. [PubMed: 15980071]

Chen J, Tu X, Esen E, Joeng KS, Lin C, Arbeit JM, Rüegg MA, Hall MN, Ma L, and Long F (2014). WNT7B promotes bone formation in part through mTORC1. PLoS Genet. 10, e1004145. [PubMed: 24497849]

Clemmons DR (1993). IGF binding proteins and their functions. Mol. Reprod. Dev. 35, 368–374, discussion 374–375. [PubMed: 7691098]

Clemmons DR (2016). Role of IGF Binding Proteins in Regulating Metabolism. Trends Endocrinol. Metab 27, 375–391. [PubMed: 27117513]

Clemmons DR (2018). Role of IGF-binding proteins in regulating IGF responses to changes in metabolism. J. Mol. Endocrinol 61, T139–T169. [PubMed: 29563157]

Clevers H, Loh KM, and Nusse R (2014). Stem cell signaling. An integral program for tissue renewal and regeneration: Wnt signaling and stem cell control. Science 346, 1248012. [PubMed: 25278615]

D'Souza RN, Aberg T, Gaikwad J, Cavender A, Owen M, Karsenty G, and Thesleff I (1999). Cbfa1 is required for epithelial-mesenchymal interactions regulating tooth development in mice. Development 126, 2911–2920. [PubMed: 10357935]

Duan C, and Xu Q (2005). Roles of insulin-like growth factor (IGF) binding proteins in regulating IGF actions. Gen. Comp. Endocrinol 142, 44–52. [PubMed: 15862547]

Feng J, Mantesso A, De Bari C, Nishiyama A, and Sharpe PT (2011). Dual origin of mesenchymal stem cells contributing to organ growth and repair. Proc. Natl. Acad. Sci. USA 108, 6503–6508. [PubMed: 21464310]

Firth SM, and Baxter RC (2002). Cellular actions of the insulin-like growth factor binding proteins. Endocr. Rev 23, 824–854. [PubMed: 12466191]

Ganz T (2000). Paneth cells—guardians of the gut cell hatchery. Nat. Immunol 1, 99–100. [PubMed: 11248797]

Gonzales KAU, and Fuchs E (2017). Skin and Its Regenerative Powers: An Alliance between Stem Cells and Their Niche. Dev. Cell 43, 387–401. [PubMed: 29161590]

Hakuno F, and Takahashi SI (2018). IGF1 receptor signaling pathways. J. Mol. Endocrinol 61, T69–T86. [PubMed: 29535161]

Heinz S, Benner C, Spann N, Bertolino E, Lin YC, Laslo P, Cheng JX, Murre C, Singh H, and Glass CK (2010). Simple combinations of lineage-determining transcription factors prime cis-regulatory elements required for macrophage and B cell identities. Mol. Cell 38, 576–589. [PubMed: 20513432]

Hsu YC, Li L, and Fuchs E (2014). Transit-amplifying cells orchestrate stem cell activity and tissue regeneration. Cell 157, 935–949. [PubMed: 24813615]

Jaruga A, Hordyjewska E, Kandzierski G, and Tylzanowski P (2016). Cleidocranial dysplasia and RUNX2-clinical phenotype-genotype correlation. Clin. Genet 90, 393–402. [PubMed: 27272193]

Jones JI, and Clemmons DR (1995). Insulin-like growth factors and their binding proteins: biological actions. Endocr. Rev 16, 3–34. [PubMed: 7758431]

Juuri E, Saito K, Ahtiainen L, Seidel K, Tummers M, Hochedlinger K, Klein OD, Thesleff I, and Michon F (2012). Sox2+ stem cells contribute to all epithelial lineages of the tooth via Sfrp5+ progenitors. Dev. Cell 23, 317–328. [PubMed: 22819339]

Kaukua N, Shahidi MK, Konstantinidou C, Dyachuk V, Kaucka M, Furlan A, An Z, Wang L, Hultman I, Ahrlund-Richter L, et al. (2014). Glial origin of mesenchymal stem cells in a tooth model system. Nature 513, 551–554. [PubMed: 25079316]

Komori T, Yagi H, Nomura S, Yamaguchi A, Sasaki K, Deguchi K, Shimizu Y, Bronson RT, Gao YH, Inada M, et al. (1997). Targeted disruption of Cbfa1 results in a complete lack of bone formation owing to maturational arrest of osteoblasts. Cell 89, 755–764. [PubMed: 9182763]

Kwon HJ, Park EK, Jia S, Liu H, Lan Y, and Jiang R (2015). Deletion of Osr2 Partially Rescues Tooth Development in Runx2 Mutant Mice. J. Dent. Res 94, 1113–1119. [PubMed: 25916343]

Lapthanasupkul P, Feng J, Mantesso A, Takada-Horisawa Y, Vidal M, Koseki H, Wang L, An Z, Miletich I, and Sharpe PT (2012). Ring1a/b polycomb proteins regulate the mesenchymal stem cell niche in continuously growing incisors. Dev. Biol. 367, 140–153. [PubMed: 22562112]

Lee HT, Chang HT, Lee S, Lin CH, Fan JR, Lin SZ, Hsu CY, Hsieh CH, and Shyu WC (2016). Role of IGF1R(+) MSCs in modulating neuroplasticity via CXCR4 cross-interaction. Sci. Rep 6, 32595. [PubMed: 27586516]

Lee JH, Tammela T, Hofree M, Choi J, Marjanovic ND, Han S, Canner D, Wu K, Paschini M, Bhang DH, et al. (2017). Anatomically and Functionally Distinct Lung Mesenchymal Populations Marked by Lgr5 and Lgr6. Cell 170, 1149–1163. [PubMed: 28886383]

Li H (2013). Aligning sequence reads, clone sequences and assembly contigs with BWA-MEM. arXiv, arXiv:1303.3997. https://arxiv.org/abs/1303.3997.

Li J, Feng J, Liu Y, Ho TV, Grimes W, Ho HA, Park S, Wang S, and Chai Y (2015). BMP-SHH signaling network controls epithelial stem cell fate via regulation of its niche in the developing tooth. Dev. Cell 33, 125–135. [PubMed: 25865348]

Li C, Jing Y, Wang K, Ren Y, Liu X, Wang X, Wang Z, Zhao H, and Feng JQ (2018). Dentinal mineralization is not limited in the mineralization front but occurs along with the entire odontoblast process. Int. J. Biol. Sci 14, 693–704. [PubMed: 29910680]

Madisen L, Zwingman TA, Sunkin SM, Oh SW, Zariwala HA, Gu H, Ng LL, Palmiter RD, Hawrylycz MJ, Jones AR, et al. (2010). A robust and high-throughput Cre reporting and characterization system for the whole mouse brain. Nat. Neurosci 13, 133–140. [PubMed: 20023653]

Miyazaki T, Kanatani N, Rokutanda S, Yoshida C, Toyosawa S, Nakamura R, Takada S, and Komori T (2008). Inhibition of the terminal differentiation of odontoblasts and their transdifferentiation into osteoblasts in Runx2 transgenic mice. Arch. Histol. Cytol 71, 131–146. [PubMed: 18974605]

Morrison SJ, and Spradling AC (2008). Stem cells and niches: mechanisms that promote stem cell maintenance throughout life. Cell 132, 598–611. [PubMed: 18295578]

Otto F, Thornell AP, Crompton T, Denzel A, Gilmour KC, Rosewell IR, Stamp GWH, Beddington RSP, Mundlos S, Olsen BR, et al. (1997). Cbfa1, a candidate gene for cleidocranial dysplasia syndrome, is essential for osteoblast differentiation and bone development. Cell 89, 765–771. [PubMed: 9182764]

Portales-Casamar E, Thongjuea S, Kwon AT, Arenillas D, Zhao X, Valen E, Yusuf D, Lenhard B, Wasserman WW, and Sandelin A (2010). JASPAR 2010: the greatly expanded open-access database of transcription factor binding profiles. Nucleic Acids Res. 38, D105–D110. [PubMed: 19906716]

Ranke MB (2015). Insulin-like growth factor binding-protein-3 (IGFBP-3). Best Pract. Res. Clin. Endocrinol. Metab 29, 701–711. [PubMed: 26522455]

Rezza A, Wang Z, Sennett R, Qiao W, Wang D, Heitman N, Mok KW, Clavel C, Yi R, Zandstra P, et al. (2016). Signaling Networks among Stem Cell Precursors, Transit-Amplifying Progenitors, and their Niche in Developing Hair Follicles. Cell Rep. 14, 3001–3018. [PubMed: 27009580]

Saito K, Takahashi K, Huang B, Asahara M, Kiso H, Togo Y, Tsukamoto H, Mishima S, Nagata M, Iida M, et al. (2018). Loss of Stemness, EMT, and Supernumerary Tooth Formation in Cebpb−/−Runx2+/− Murine Incisors. Sci. Rep 8, 5169. [PubMed: 29581460]

Satija R, Farrell JA, Gennert D, Schier AF, and Regev A (2015). Spatial reconstruction of single-cell gene expression data. Nat. Biotechnol 33, 495–502. [PubMed: 25867923]

Sato T, van Es JH, Snippert HJ, Stange DE, Vries RG, van den Born M, Barker N, Shroyer NF, van de Wetering M, and Clevers H (2011). Paneth cells constitute the niche for Lgr5 stem cells in intestinal crypts. Nature 469, 415–418. [PubMed: 21113151]

Scadden DT (2014). Nice neighborhood: emerging concepts of the stem cell niche. Cell 157, 41–50. [PubMed: 24679525]

Seidel K, Ahn CP, Lyons D, Nee A, Ting K, Brownell I, Cao T, Carano RA, Curran T, Schober M, et al. (2010). Hedgehog signaling regulates the generation of ameloblast progenitors in the continuously growing mouse incisor. Development 137, 3753–3761. [PubMed: 20978073]

Sharpe PT (2016). Dental mesenchymal stem cells. Development 143, 2273–2280. [PubMed: 27381225]

Shi C, Yuan Y, Guo Y, Jing J, Ho TV, Han X, Li J, Feng J, and Chai Y (2019). BMP Signaling in Regulating Mesenchymal Stem Cells in Incisor Homeostasis. J. Dent. Res 98, 904–911. [PubMed: 31136721]

Simons BD, and Clevers H (2011). Strategies for homeostatic stem cell self-renewal in adult tissues. Cell 145, 851–862. [PubMed: 21663791]

Song J, Zhong C, Bonaguidi MA, Sun GJ, Hsu D, Gu Y, Meletis K, Huang ZJ, Ge S, Enikolopov G, et al. (2012). Neuronal circuitry mechanism regulating adult quiescent neural stem-cell fate decision. Nature 489, 150–154. [PubMed: 22842902]

Takarada T, Hinoi E, Nakazato R, Ochi H, Xu C, Tsuchikane A, Takeda S, Karsenty G, Abe T, Kiyonari H, and Yoneda Y (2013). An analysis of skeletal development in osteoblast-specific and chondrocyte-specific runt-related transcription factor-2 (Runx2) knockout mice. J. Bone Miner. Res 28, 2064–2069. [PubMed: 23553905]

Tammela T, Sanchez-Rivera FJ, Cetinbas NM, Wu K, Joshi NS, Helenius K, Park Y, Azimi R, Kerper NR, Wesselhoeft RA, et al. (2017). A Wnt-producing niche drives proliferative potential and progression in lung adenocarcinoma. Nature 545, 355–359. [PubMed: 28489818]

van Velthoven CTJ, and Rando TA (2019). Stem Cell Quiescence: Dynamism, Restraint, and Cellular Idling. Cell Stem Cell 24, 213–225. [PubMed: 30735649]

Wang XP, Suomalainen M, Felszeghy S, Zelarayan LC, Alonso MT, Plikus MV, Maas RL, Chuong CM, Schimmang T, and Thesleff I (2007). An integrated gene regulatory network controls stem cell proliferation in teeth. PLoS Biol. 5, e159. [PubMed: 17564495]

Wang S, Zhang S, Wang Y, Chen Y, and Zhou L (2013). Cleidocranial dysplasia syndrome: clinical characteristics and mutation study of a Chinese family. Int. J. Clin. Exp. Med 6, 900–907. [PubMed: 24260595]

Wu H, Whitfield TW, Gordon JA, Dobson JR, Tai PW, van Wijnen AJ, Stein JL, Stein GS, and Lian JB (2014). Genomic occupancy of Runx2 with global expression profiling identifies a novel dimension to control of osteoblastogenesis. Genome Biol. 15, R52. [PubMed: 24655370]

Xian L, Wu X, Pang L, Lou M, Rosen CJ, Qiu T, Crane J, Frassica F, Zhang L, Rodriguez JP, et al. (2012). Matrix IGF-1 maintains bone mass by activation of mTOR in mesenchymal stem cells. Nat. Med 18, 1095–1101. [PubMed: 22729283]

Yang H, Adam RC, Ge Y, Hua ZL, and Fuchs E (2017). Epithelial-Mesenchymal Micro-niches Govern Stem Cell Lineage Choices. Cell 169, 483–496. [PubMed: 28413068]

Youssef A, Aboalola D, and Han VK (2017). The Roles of Insulin-Like Growth Factors in Mesenchymal Stem Cell Niche. Stem Cells Int. 2017, 9453108. [PubMed: 28298931]

Zhang Y, Liu T, Meyer CA, Eeckhoute J, Johnson DS, Bernstein BE, Nusbaum C, Myers RM, Brown M, Li W, and Liu XS (2008). Model-based analysis of ChIP-Seq (MACS). Genome Biol. 9, R137. [PubMed: 18798982]

Zhao H, Feng J, Seidel K, Shi S, Klein O, Sharpe P, and Chai Y (2014). Secretion of shh by a neurovascular bundle niche supports mesenchymal stem cell homeostasis in the adult mouse incisor. Cell Stem Cell 14, 160–173. [PubMed: 24506883]

Ziegler AN, Feng Q, Chidambaram S, Testai JM, Kumari E, Rothbard DE, Constancia M, Sandovici I, Cominski T, Pang K, et al. (2019). Insulin-like Growth Factor II: An Essential Adult Stem Cell Niche Constituent in Brain and Intestine. Stem Cell Reports 12, 816–830. [PubMed: 30905741]

Highlights

- MSCs are heterogeneous in the adult mouse incisor
- Runx2+/Gli1+ cells are MSC niche cells, but not MSCs
- Runx2+/Gli1+ cells coordinate the MSC-to-TAC transition and the incisor growth rate
- Runx2-mediated IGF signaling controls cell fate of TACs

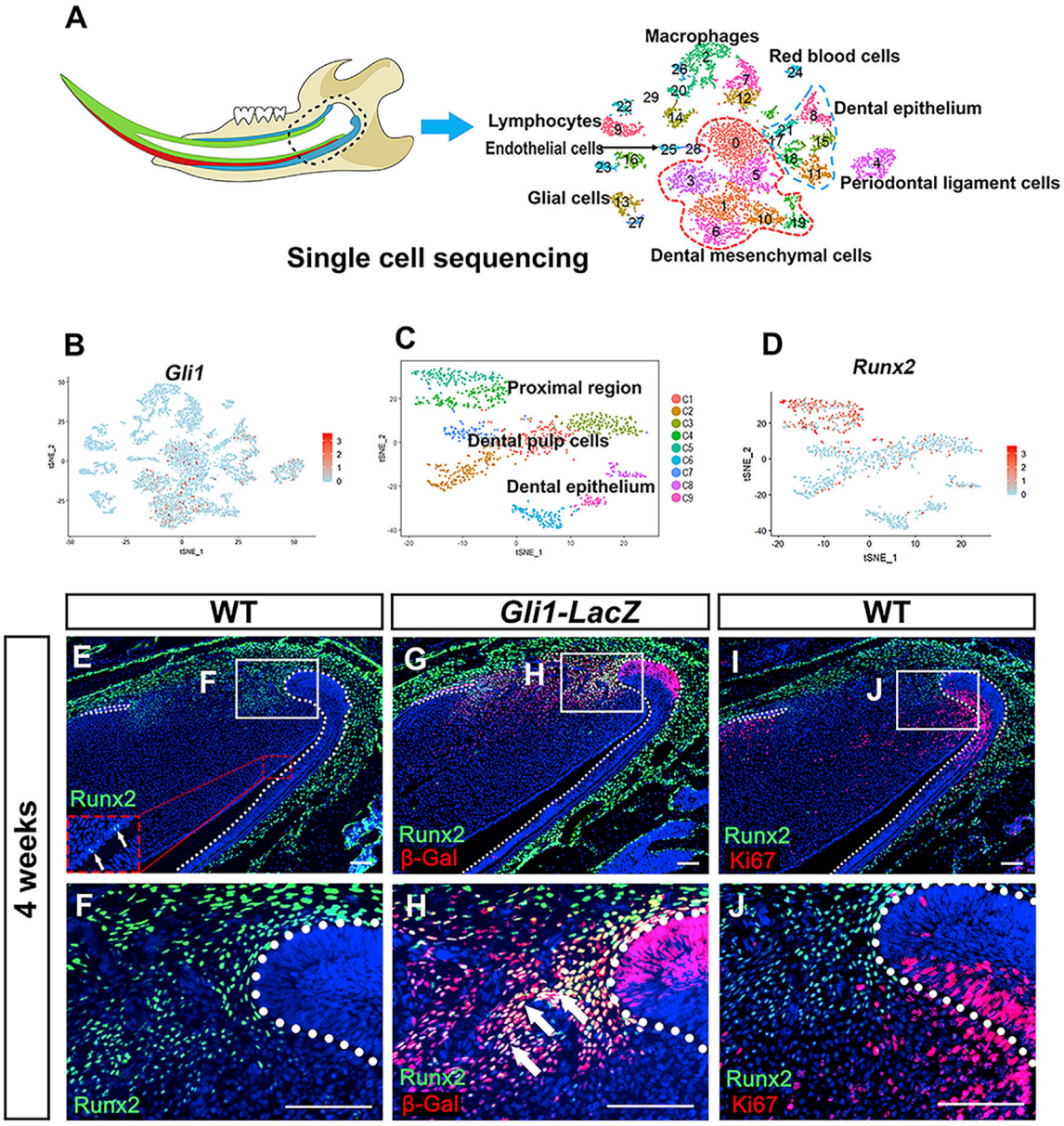

Figure 1. Runx2 Is Expressed in a Subpopulation of Gli1+ Cells in the Proximal Region of the Incisor

(A) Unbiased t-SNE plots of cell clusters in the incisor from 1-month-old wild-type mice. The schematic shows the location from which the tissue was harvested.

The red dotted line marks dental mesenchyme, and the blue dotted line marks dental epithelium.

(B) t-SNE plot showing the expression of *Gli1* in different clusters of the mouse incisor.

(C) Subpopulations of Gli1+ cells re-clustered by t-SNE analysis.

(D) t-SNE plot showing expression of *Runx2* in Gli1+ subclusters.

(E and F) Runx2 immunostaining of a 1-month-old wild-type (WT) mouse. (F) High-magnification image of the inset in (E). Runx2 expression in odontoblasts is shown in the red box in (E).

(G and H) Runx2 and β-galactosidase (β-gal) double immunostaining of incisor from a 1-month-old *Gli1-LacZ* mouse. (H) High-magnification image of the inset in (G). Arrows show colocalization of Runx2+ cells and Gli1+ cells.
(I and J) Runx2 and Ki67 double immunostaining of incisor from a 1-month-old wild-type mouse. (J) High-magnification image of the inset in (I).
The white dotted line in (E)–(J) shows the cervical loop. Scale bars, 100 μm.

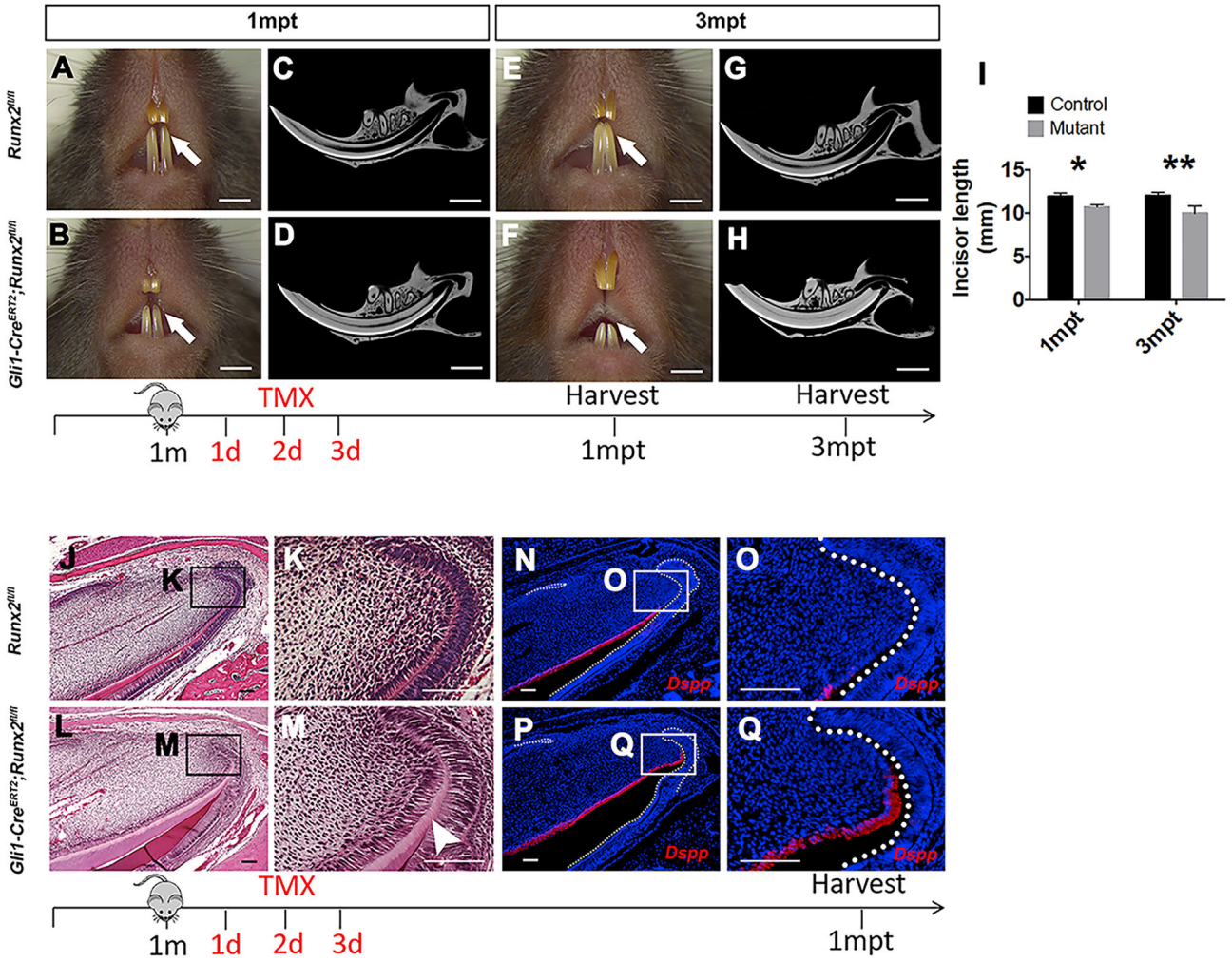

Figure 2. Loss of Runx2 in the Gli1+ Lineage Impairs the Incisor Growth Rate

(A and B) Gross appearance of incisors from *Runx2*$^{fl/fl}$ mice (A) and *Gli1-Cre*^{ERT2};*Runx2*$^{fl/fl}$ mice (B) 1 month after tamoxifen induction (mpt) at 1 month of age. Arrows point to the lower incisors.

(C and D) Longitudinal micro-CT images from 1-month-old *Runx2*$^{fl/fl}$ mice (C) and *Gli1-Cre*^{ERT2};*Runx2*$^{fl/fl}$ mice (D) 1 mpt.

(E and F) Gross appearance of incisors from *Runx2*$^{fl/fl}$ mice (E) and *Gli1-Cre*^{ERT2};*Runx2*$^{fl/fl}$ mice (F) 3 mpt at 1 month of age. Arrows point to the lower incisors.

(G and H) Longitudinal micro-CT images from 1-month-old *Runx2*$^{fl/fl}$ mice (G) and *Gli1-Cre*^{ERT2};*Runx2*$^{fl/fl}$ mice (H) 3 mpt.

(I) Comparison of the incisor lengths of *Runx2*$^{fl/fl}$ (control) and *Gli1-Cre*^{ERT2};*Runx2*$^{fl/fl}$ (mutant) mice 1 and 3 months after induction at 1 month of age. n = 5 mice, *p < 0.05, **p < 0.01.

(J–M) Histological analysis of incisors from *Runx2*$^{fl/fl}$ mice (J and K) and *Gli1-Cre*^{ERT2};*Runx2*$^{fl/fl}$ mice (L and M) 1 mpt at 1 month of age. (K) and (M) High-magnification images of the insets in (J) and (L), respectively. The arrowhead in (M) indicates abnormal dentin formation.

(N–Q) *Dspp* RNAscope of incisors from *Runx2*$^{fl/fl}$ (N) and *Gli1-Cre*^{ERT2};*Runx2*$^{fl/fl}$ mice (P) 1 mpt at 1 month of age. (O) and (Q) High-magnification images of the insets in (N) and (P), respectively. The white dotted line shows the cervical loop.

The schematic at the bottom of each set of panels indicates the induction protocol. Data are represented as mean ± SEM. TMX, tamoxifen. Scale bars, (A–H) 2 mm, (J–Q) 100 μm.

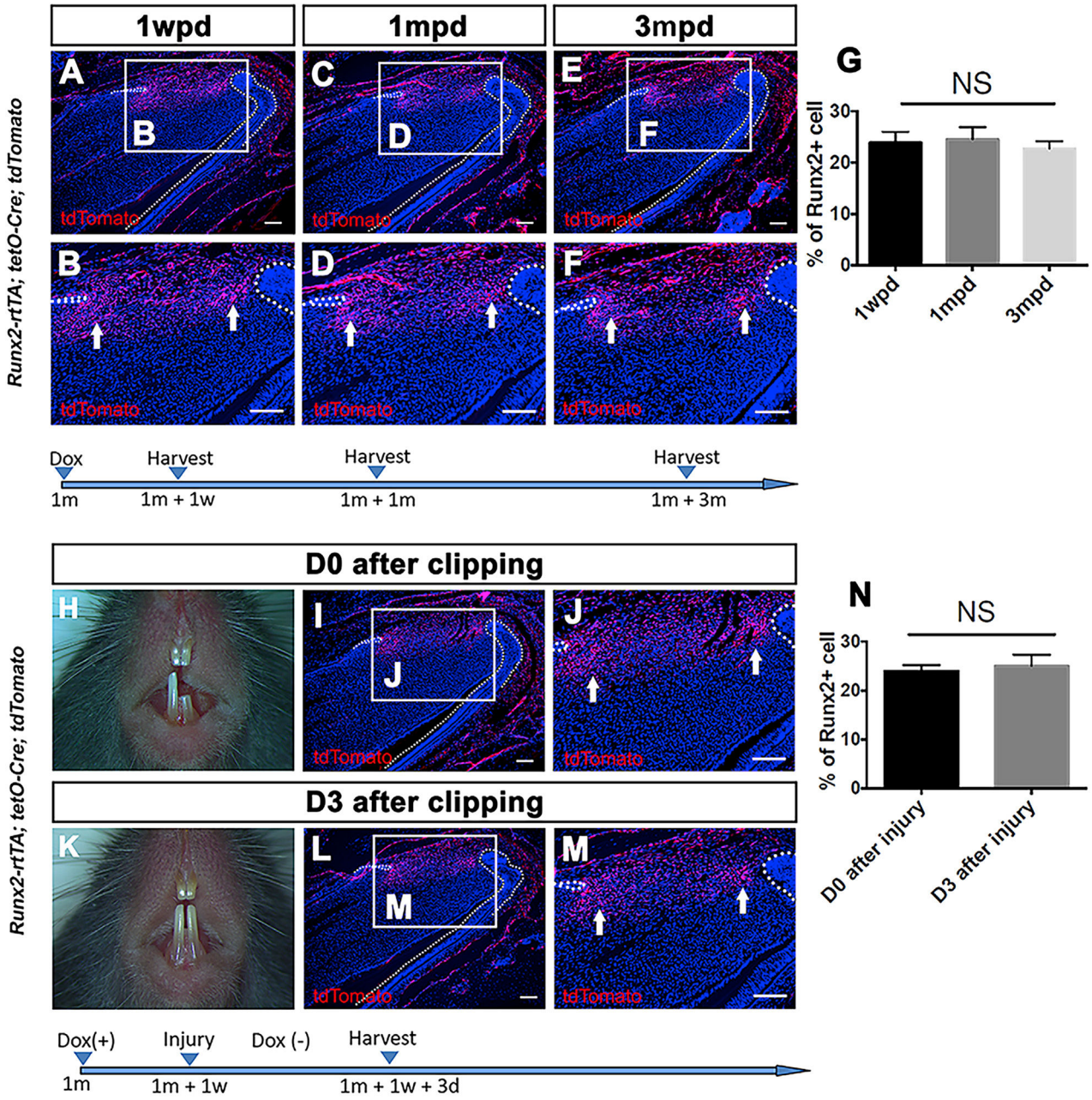

Figure 3. Runx2+ Cells Are Niche Cells that Maintain Tissue Homeostasis in the Mouse Incisor

(A and B) tdTomato immunostaining of incisors from *Runx2-rtTA;tetO-Cre;tdTomato* mice 1 week after doxycycline induction (wpd) at one month of age. (B) High-magnification image of the inset in (A).

(C and D) tdTomato immunostaining of incisors from *Runx2-rtTA;tetO-Cre;tdTomato* mice 1 month after doxycycline induction (mpd) at one month of age. (D) High-magnification image of the inset in (C).

(E and F) tdTomato immunostaining of incisors from *Runx2-rtTA;tetO-Cre;tdTomato* mice 3 mpd at one month of age. (F) High-magnification image of the inset in (E).

(G) Quantification analysis of the percentage of Runx2+ cells per high-magnification section (B, D, and F) 1 week, 1 month, and 3 months after induction of the *Runx2-rtTA;tetO-Cre;tdTomato* incisor mesenchyme. n = 3 mice/group.

(H) Gross appearance of incisors from a 1-month-old *Runx2-rtTA;tetO-Cre;tdTomato* mouse on day 0 after clipping, which took place 1 wpd at one month of age.

(I and J) tdTomato immunostaining of incisors from *Runx2-rtTA;tetO-Cre;tdTomato* mice on day 0 after clipping. (J) High-magnification image of the inset in (I).

(K) Gross appearance of incisors from a 1-month-old *Runx2-rtTA;tetO-Cre;tdTomato* mouse on day 3 after clipping. Mice were served doxycycline-free food after clipping.

(L and M) tdTomato immunostaining of incisors from *Runx2-rtTA;tetO-Cre;tdTomato* mice on day 3 after clipping. (M) High-magnification image of the inset in (L).

(N) Quantification analysis of the percentage of Runx2+ cells per high-magnification section (J and M) days 0 and 3 after clipping of the *Runx2-rtTA;tetO-Cre;tdTomato* incisor mesenchyme. n = 3 mice/group.

NS, no significant difference; Dox, doxycycline. The schematic at the bottom of each set of panels indicates the induction protocol. The white dotted line in (A)–(F), (I), (J), (L), and (M) shows the cervical loop. Arrows shows tdTomato signaling in the proximal region. All data are represented as mean ± SEM. Scale bars, 100 μm.

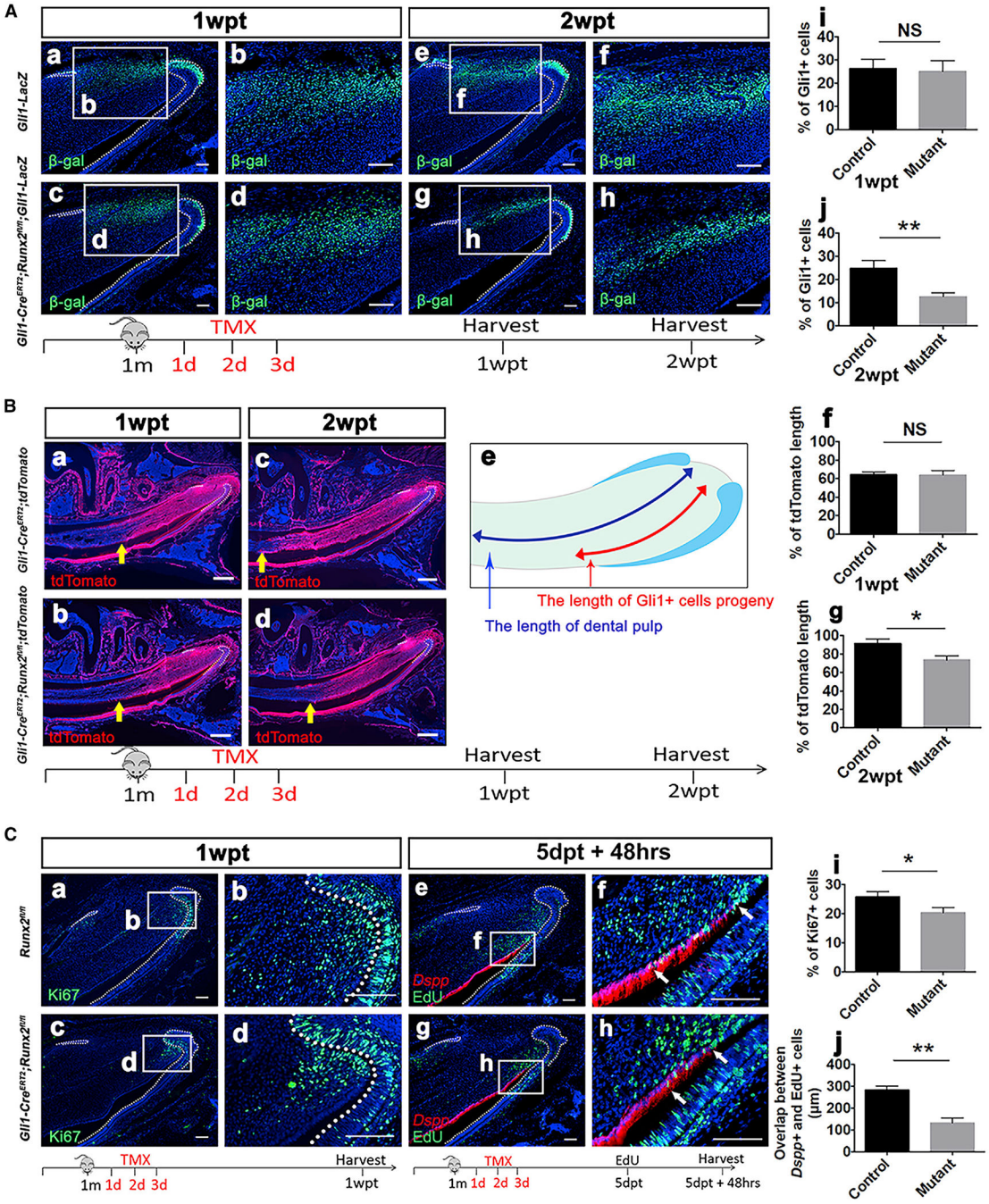

Figure 4. Runx2+ Cells Maintain the Incisor MSC Niche by Regulating TAC Proliferation and Differentiation

(A) β-gal staining of incisor from *Gli1-LacZ* and *Gli1-Cre*^{ERT2};*Runx2*$^{fl/fl}$;*Gli1-LacZ* mice one week (a and c) and two weeks (e and g) after induction. (b, d, f, and h) High-magnification images of the insets in (a), (c), (e), and (g), respectively. (i and j) Quantification of the percentage of Gli1+ cells per high-magnification section (b, d, f, and h) one week (i) and two weeks (j) after induction of the *Gli1-LacZ* and *Gli1-Cre*^{ERT2};*Runx2*$^{fl/fl}$;*Gli1-LacZ* incisor mesenchyme.

(B) Differentiation rate of Gli1+ MSCs in *Gli1-Cre^{ERT2};tdTomato* and *Gli1-Cre^{ERT2};Runx2$^{fl/fl}$;tdTomato* mice one week (a and b) and two weeks (c and d) after induction. (e) Schematic showing the method of measuring the length of the tdTomato signal and dental pulp. (f and g) Quantification of the percentage of tdTomato signal one week (f) and two weeks (g) after induction of *Gli1-Cre^{ERT2};tdTomato* and *Gli1-Cre^{ERT2};Runx2$^{fl/fl}$;tdTomato* mice.

(C) Ki67 immunostaining of incisors from 1-month-old *Runx2$^{fl/fl}$* mice (a) and *Gli1-Cre^{ERT2};Runx2$^{fl/fl}$* mice (c) one week after induction. (b and d) High-magnification images of the insets in (a) and (c), respectively. (e and g) RNAscope of *Dspp* and EdU staining in *Runx2$^{fl/fl}$* mice (e) and *Gli1-Cre^{ERT2};Runx2$^{fl/fl}$* mice (g) one week after induction. (f and h) High-magnification images of the insets in (e) and (g), respectively. (i) Quantification analysis of the percentage of Ki67+ cells per high-magnification section (b and d) one week after induction of the *Runx2$^{fl/fl}$* and *Gli1-Cre^{ERT2};Runx2$^{fl/fl}$* incisor mesenchyme. (j) Quantification analysis of the length of overlap between *Dspp*+ and EdU+ cells (f and h) one week after induction of *Runx2$^{fl/fl}$* and *Gli1-Cre^{ERT2};Runx2$^{fl/fl}$* incisor.

n = 3 mice/group. NS, no significant difference. *$p < 0.05$, **$p < 0.01$. The schematic at the bottom of each group of subpanels shows tamoxifen induction and EdU injection protocols. The white dotted line shows the cervical loop. All data are represented as mean ± SEM. Scale bars, (A and C) 100 μm, (B) 500 μm.

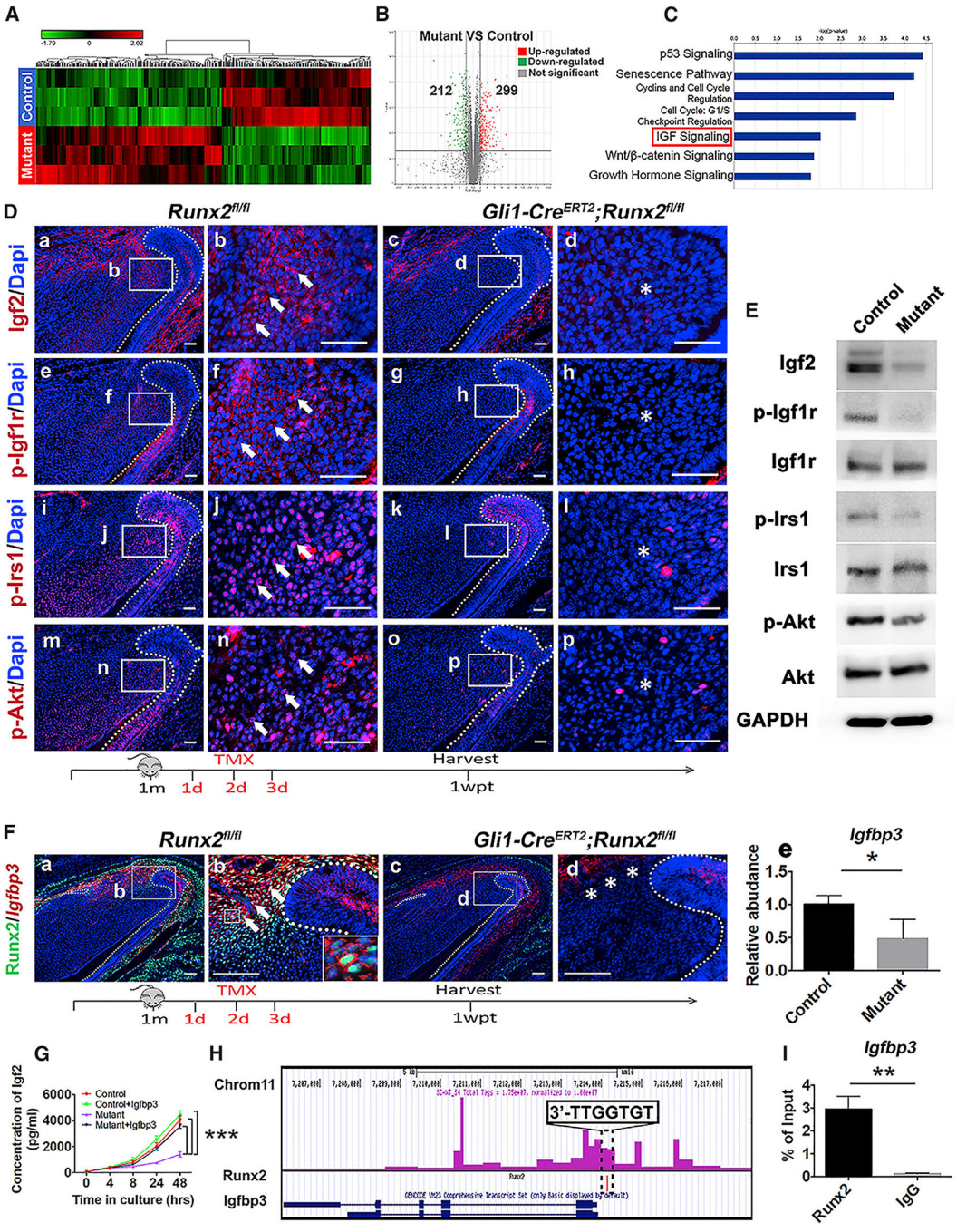

Figure 5. IGF-2 Signaling Is Downregulated in *Gli1-Cre*^{ERT2};*Runx2*$^{fl/fl}$ Mice

(A) Heatmap hierarchical clustering showing the gene expression profiles of *Runx2*$^{fl/fl}$ (control) and *Gli1-Cre*^{ERT2};*Runx2*$^{fl/fl}$ (mutant) mice one week after induction at one month of age.

(B) Volcano plot revealing that 299 genes were upregulated and 212 genes were downregulated (>2-fold, $p < 0.05$) in *Gli1-Cre*^{ERT2};*Runx2*$^{fl/fl}$ mice.

(C) IPA based on RNA-seq data.

(D) Immunostaining of Igf2 (a and c), p-Igf1r (e and g), p-Irs1 (i and k), and p-Akt (m and o) in incisors from *Runx2*$^{fl/fl}$ mice (a, e, i, and m) and *Gli1-Cre*^{ERT2};*Runx2*$^{fl/fl}$ mice (c, g, k, and o) 1 week after induction at 1 month of age. (b, d, f, h, j, l, n, and p) High-magnification images of the insets in (a), (c), (e), (g), (i), (k), (m), and (o), respectively. Arrows indicate a positive signal, and asterisks indicate the absence of a signal.

(E) Western blot of Igf2, p-Igf1r, Igf1r, p-Irs1, Irs1, p-Akt, and Akt in the incisor mesenchyme from *Runx2*$^{fl/fl}$ (control) and *Gli1-Cre*^{ERT2};*Runx2*$^{fl/fl}$ (mutant) mice one week after induction.

(F) *Igfbp3* RNAscope and Runx2 immunostaining of incisor from *Runx2*$^{fl/fl}$ mice (a) and *Gli1-Cre*^{ERT2};*Runx2*$^{fl/fl}$ mice (c) 1 week after induction at 1 month of age. (b and d) High-magnification images of the insets in (a) and (c), respectively. (e) Real-time PCR analysis of *Igfbp3* in the incisor mesenchyme from *Runx2*$^{fl/fl}$ and *Gli1-Cre*^{ERT2};*Runx2*$^{fl/fl}$ mice 1 week after induction at 1 month of age. n = 3/group, *$p < 0.05$. Arrows indicate coexpression of the *Igfbp3* mRNA and Runx2 protein, and asterisks indicate the absence of a signal.

(G) ELISA showing the secreted Igf2 in the culture medium supernatant from the MSCs of *Runx2*$^{fl/fl}$ (control) and *Gli1-Cre*^{ERT2};*Runx2*$^{fl/fl}$ (mutant) mice with or without Igfbp3 protein. n = 3, ***$p < 0.001$.

(H) ATAC-seq analysis of the incisor mesenchyme from 1-month-old wild-type mice. The black box indicates the Runx2 binding motif located at the promoter of *Igfbp3*.

(I) ChIP with Runx2 antibody (or immunoglobulin G [IgG]), followed by qPCR to compare levels of Runx2 the near transcription start site of *Igfbp3*, in the incisor mesenchyme from 1-month-old wild-type mice. n = 4, **$p < 0.01$.

The schematic at the bottom of each group of subpanels shows tamoxifen induction protocols. The white dotted line in (D) and (F) shows the cervical loop. All data are represented as mean ± SEM. Scale bars, (D) 50 μm, (F) 100 μm.

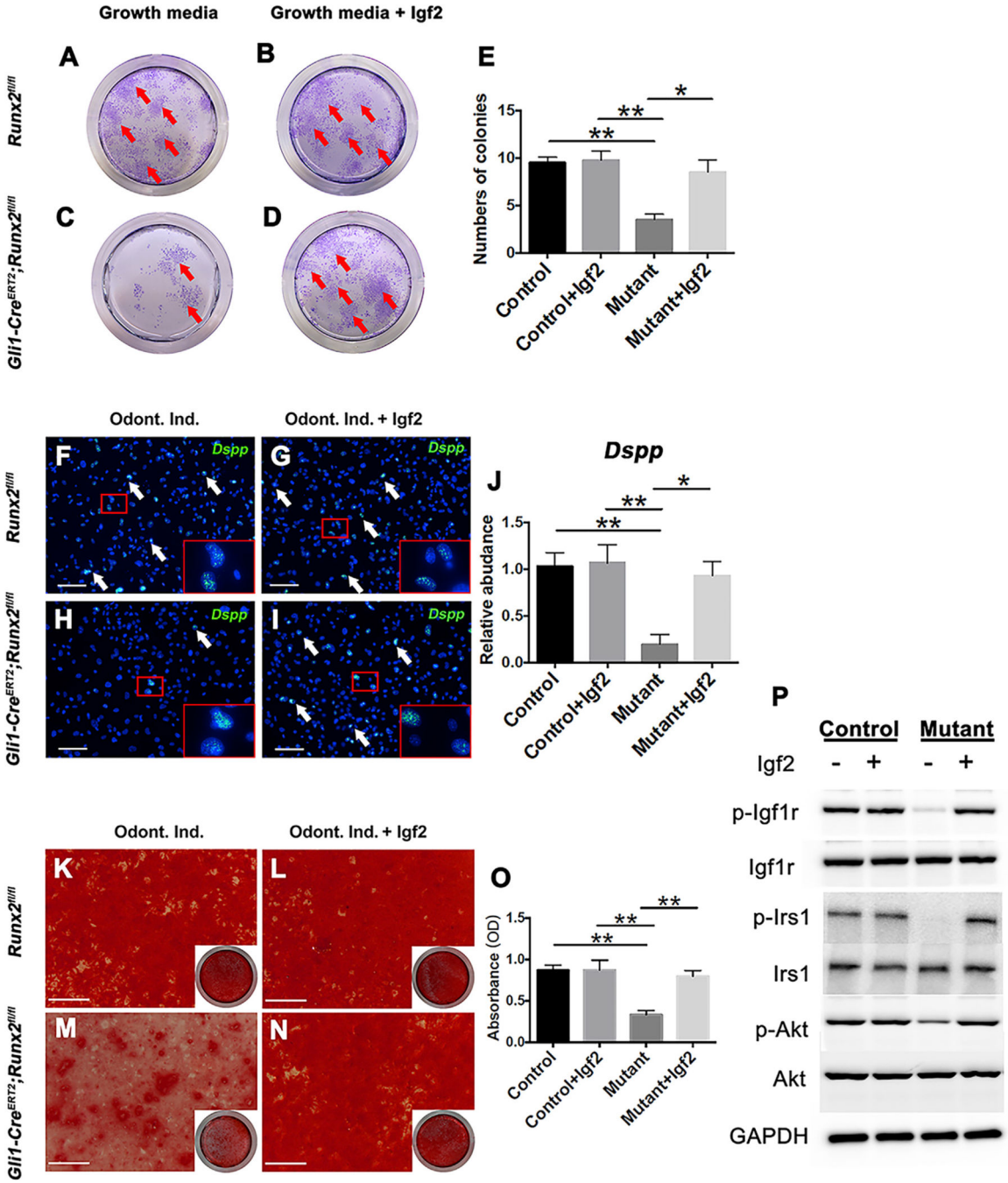

Figure 6. Igf2 Rescues Proliferation and Odontogenic Differentiation of MSCs from *Gli1-Cre^{ERT2};Runx2$^{fl/fl}$* Mice *In Vitro*

(A–D) Colony formation of MSCs from *Runx2$^{fl/fl}$* (A and B) and *Gli1-Cre^{ERT2};Runx2$^{fl/fl}$* (C and D) incisors with (B and D) or without (A and C) Igf2. Arrows indicate colony formation.

(E) Quantification of the colony formation of MSCs from *Runx2$^{fl/fl}$* and *Gli1-Cre^{ERT2};Runx2$^{fl/fl}$* incisors. n = 3, *p < 0.05, **p < 0.01.

(F–I) *Dspp* RNAscope of MSCs from *Runx2*$^{fl/fl}$ (F and G) and *Gli1-Cre*^{ERT2};*Runx2*$^{fl/fl}$ (H and I) incisors 1 week after odontogenic induction (Odont. Ind.) with (G and I) or without (F and H) Igf2 protein.

(J) Real-time PCR analysis of *Dspp* after odontogenic induction. n = 3, *p < 0.05, **p < 0.01.

(K–N) Alizarin red staining of the MSCs from *Runx2*$^{fl/fl}$ (K and L) and *Gli1-Cre*^{ERT2};*Runx2*$^{fl/fl}$ (M and N) incisors 3 weeks after odontogenic induction with (L and N) or without (K and M) Igf2 protein.

(O) Absorbance analysis of the dissolved Alizarin red contents at 590 nm. n = 3, **p < 0.01.

(P) Western blot of p-Igf1r, Igf1r, p-Irs1, Irs1, p-Akt, and Akt of the MSCs from *Runx2*$^{fl/fl}$ (control) and *Gli1-Cre*^{ERT2};*Runx2*$^{fl/fl}$ (mutant) incisors 1 week after odontogenic induction with or without Igf2 protein.

All data are represented as mean ± SEM. Scale bars, (F–I) 100 μm, (K–N) 500 μm.

KEY RESOURCES TABLE

REAGENT or RESOURCE	SOURCE	IDENTIFIER
Antibodies		
Rabbit anti-Ki67	Abcam	Cat# ab15580; RRID:AB_443209
Chicken Anti-beta Galactosidase	Abcam	Cat# ab9361; RRID:AB_307210
Rabbit anti-Runx2 (D1L7F)	Cell Signaling Technology	Cat# 12556; RRID:AB_2732805
Goat polyclonal to IGF-2	Abcam	Cat# Ab123812; RRID: AB_10972691
Rabbit anti-Phospho-IGF1 Receptor	Abcam	Cat# ab39398; RRID:AB_731544
Rabbit anti-Phospho-IRS-1 (Ser612)	Cell Signaling Technology	Cat# 3203; RRID:AB_1031167
Rabbit anti-Phospho-Akt (Ser473)	Cell Signaling Technology	Cat# 4060; RRID:AB_2315049
Rabbit Anti-IGF2	Abcam	Cat# Ab262713
Rabbit anti-IGF-I Receptor β	Cell Signaling Technology	Cat# 3027; RRID:AB_2122378
Rabbit anti-Phospho-IGF-I Receptor β (Tyr1131)	Cell Signaling Technology	Cat# 3021; RRID:AB_331578
Rabbit anti-IRS-1	Cell Signaling Technology	Cat# 2382; RRID:AB_330333
Rabbit anti-Akt	Cell Signaling Technology	Cat# 9272; RRID:AB_329827
Rabbit anti-GAPDH (D16H11) XP	Cell Signaling Technology	Cat# 5174; RRID:AB_10622025
Rabbit Anti-Cytokeratin 14	Abcam	Cat# ab181595; RRID:AB_2811031
Alexa Fluor 594 Tyramide SuperBoost Kit, goat anti-rabbit IgG	Thermo Fisher Scientific	Cat# B40925
Goat anti-Rabbit IgG (H+L) Cross-Adsorbed Secondary Antibody, Alexa Fluor 488,	Thermo Fisher Scientific	Cat# A-11008; RRID:AB_143165
Goat anti-Rabbit IgG (H+L) Cross-Adsorbed Secondary Antibody, Alexa Fluor 568	Thermo Fisher Scientific	Cat# A-11011; RRID:AB_143157
Chicken anti-Goat IgG (H+L) Secondary Antibody	Thermo Fisher Scientific	Cat# A15963; RRID:AB_2534637
Chemicals, Peptides, and Recombinant Proteins		
Tamoxifen	Sigma-Aldrich	Cat# T5648-5G
Rodent Diet (2018, 625 Dox, R)	ENVIGO	Cat# TD.08541
Fetal Bovine Serum	Thermo Fisher Scientific	Cat# 26140095
α-MEM	Thermo Fisher Scientific	Cat# 12571-048
Collagenase, Type 1	Worthington	Cat# LS004194
Recombinant Mouse Igfbp3 protein,CF	R&D Systems	Cat# 775-B3
Insulin-like Growth Factor-II from mouse	Sigma-Aldrich	Cat# I8904
RIPA Buffer (10X)	Cell Signaling Technology	Cat# 9806s
Protease inhibitor	ThermoFisher Scientific,	Cat# A32959
DAPI Solution (1 mg/mL)	Thermo Fisher Scientific	Cat# 62248
Dexamethasone	Sigma-Aldrich	Cat# D4902-25MG
Ascorbic acid	Sigma-Aldrich	Cat# 1043003-1G
β-Glycerol phosphate disodium salt pentahydrate	Sigma-Aldrich	Cat# 50020-100G
Alizarin Red S	ACROS Organics	Cat# 400480250
Toluidine Blue O	Sigma-Aldrich	Cat# T3260
Critical Commercial Assays		

REAGENT or RESOURCE	SOURCE	IDENTIFIER
Click-iT Plus TUNEL Assay for *In Situ* Apoptosis Detection, Alexa Fluor 488 dye	Thermo Fisher Scientific	Cat# C10617
Click-iT Plus EdU Cell Proliferation Kit for Imaging, Alexa Fluor 488 dye	Thermo Fisher Scientific	Cat# C10637
RNeasy Micro Kit	QIAGEN	Cat#74004
RNAscope® Multiplex Fluorescent v2	ACD	Cat#323100
Probe- Mm-Igf2	ACD	Cat#437671
Probe- Mm-Igfbp1	ACD	Cat#530371
Probe- Mm-Igfbp2	ACD	Cat#405951
Probe- Mm-Igfbp3	ACD	Cat#405941
Probe- Mm-Igfbp4	ACD	Cat#425711
Probe- Mm-Igfbp5	ACD	Cat#425731
Probe- Mm-Igfbp6	ACD	Cat#425721
Probe- Mm-Dspp	ACD	Cat#448301
Probe- Mm-Smoc2	ACD	Cat#318541
Probe- Mm-Sox9	ACD	Cat #401051
TSA Plus Cyanine 3 System	Perkin Elmer	Cat#NEL744001KT
Chromium Single Cell 3′ GEM, Library & Gel Bead Kit v3	10× Genomics Inc.	Cat#1000092
iScript cDNA Synthesis Kit	Bio-Rad	Cat#1708890
SsoFast EvaGreen® Supermix	Bio-Rad	Cat#1725202
Chromatrap Enzymatic ChIP-seq Protein A	Chromatrap	Cat#500191
Mouse/Rat/Porcine/Canine IGF-II/IGF2 Quantikine ELISA Kit	R&D Systems	Cat#MG200
Deposited Data		
scRNA-seq data	This paper	GEO: GSE154158
Bulk RNA-seq data	This paper	GEO: GSE154158
ATAC-seq data	This paper	GEO: GSE154158
Experimental Models: Organisms/Strains		
Mouse:C57BL/6J	Jackson Laboratory	JAX:000664; RRID: IMSR_JAX:000664
Mouse:*Gli1*$^{cre/ERT2}$:STOCK *Gli1*$^{tm3(cre/ERT2)Alj}$	Jackson Laboratory	JAX:007913; RRID: IMSR_JAX:007913
Mouse: *Gli1-LacZ*:STOCK Gli1tm2Alj/J	Jackson Laboratory	JAX:008211; RRID: IMSR_JAX:008211
Mouse: *ROSA26*$^{loxp\text{-}STOP\text{-}loxp\text{-}tdTomato}$:B6;129S6-Gt(ROSA)26Sor$^{tm9(CAG\text{-}tdTomato)Hze}$/J	Jackson Laboratory	JAX:007905; RRID: IMSR_JAX:007905
Mouse: *Sox2*$^{cre/ERT2}$:B6;129S-*Sox2*$^{tm1(cre/ERT2)Hoch}$/J	Jackson Laboratory	JAX:017593; RRID: IMSR_JAX:017593
Mouse: tetO-cre: B6.Cg-Tg(tetO-cre)1Jaw/J	Jackson Laboratory	JAX:006234; RRID: IMSR_JAX:006234
Mouse: *Runx2-rtTA*	Chen et al., 2014	N/A
Mouse: *Runx2*$^{flox/flox}$	Takarada et al., 2013	N/A
Oligonucleotides		
Primer sequences	See Table S2	N/A

REAGENT or RESOURCE	SOURCE	IDENTIFIER
Software and Algorithms		
ImageJ	NIH	RRID: SCR_003070
GraphPad Prism	GraphPad Software	RRID: SCR_002798